Uppsala University

Master Thesis

Mass limits for five-dimensional super Yang-Mills

Author:
Umberto Borla

Supervisor:
Prof. J. Minahan

November 2014

FYSMAS1022

UPPSALA UNIVERSITY

Abstract

Faculty of Science and Technology
Department of Theoretical Physics

Master of Science

by Umberto Borla

In this thesis we consider the $N = 1$ super Yang-Mills theory on S^5 with a single hypermultiplet in the adjoint representation. We argue that there is a critical value of the hypermultiplet mass $M = \frac{3}{2r}$, where r is the radius of S^5, for which the free energy vanishes, and we study the model in the proximity of this value. For large N we provide analytical results for the free energy and the eigenvalue density in the weak and strong coupling limits, and in one case we solve the saddle point equation using a technique introduced by Hoppe. We present numerical results to show where each approximation is justified, and to explore the regimes where the model cannot be solved analytically. Based on the numerical results, we argue that in most cases the behaviour of the model is better understood in terms of an effective coupling constant $\bar{\lambda} = \lambda M$. For small M the model simplifies to one whose kernel is non-singular. This simplified model shows a peculiar peak structure in the eigenvalue distribution, with the number of peaks growing as the effective coupling is increased. We interpret this as a series of phase transitions as M approaches $\frac{3}{2r}$.

Populärvetenskaplig sammanfattning

En av de vägledande principerna i modern fundamental fysik är symmetri. Närvaron av en symmetri i systemet tillåter generellt sett att man kan studera det enklare: system som har en symmetri besitter färre frihetsgrader än liknande system som inte har symmetrin. Å andra sidan, om vi vet, eller vi antar, att några fenomen bör vara symmetriska med avseende på vissa transformationer, är det lättare för oss att formulera en teori som beskriver dessa fenomen, eftersom teorin kommer att bli mer bägrensad. Teorierna som beskriver de grundläggande växelverkningarna i vårt universum görs med antagandet att det finns två symmetrier: Poincaré invarians och gauge invarians. I syfte att utvidga och förbättra Standardmodellen har en ny symmetri introducerats; den så kallade supersymmetrin (SUSY). Till skillnad från de tidigare två symmetrierna, relaterar denna symmetri partiklar med heltal spin till partiklar med halv heltal spin, och förutspår " superpartners " för var och en av de redan observerade partiklarna. Även om det inte har bekräftats ännu är SUSY en av de dominerande forskningsområdena i partikelfysik, på grund av dess tilltalande fysiska egenskaper och intressanta matematiska egenskaper. Ett stort utbud av supersymmetriska teorier finns, några av dem är ganska realistiska och kan lösa en del av de problem som uppstått i standardmodellen, medan andra är mer exotiska och kan inte vara direkt relaterade till partikelfysiken. Bland dessa finns det mycket intressanta teorierna som definieras på böjda ytor t.ex. sfärer och tori. Det är intressanta på grund av de icke-triviala egenskaper som uppstår från dessa strukturer. I vissa fall är supersymmetri så begränsande att rumtidens frihetsgrader inte kommer fram i beräkningen av några fysiska kvantiteter, som istället endast är beroende av vissa specifika delar i teorin. När detta händer säger vi att teorin "lokaliseras ". I denna avhandling undersöker vi en supersymmetrisk teori definierad på en fem-dimensionell sfär. Dess beteende undersöks genom att studera en motsvarande matrismodell, det vill säga en lokaliserad version av dess partitionsfunktionen. I de tre första kapitlen ges en allmän introduktion till matrismodeller och supersymmetri i 5 dimensioner, medan kapitel 4 innehåller studien av matrismodellens olika gränser. Från denna analys visar det sig att modellen visar ganska intressanta egenskaper när massan av en av partiklarna närmar sig ett visst speciellt värde som relaterat till radien för 5-sfären. Bland dessa egenskaper är det särskilt intressant att modellen genomgår en fasövergång, det vill säga en variation av beteendet av dess lösningar, när kopplingskonstanten ökas och massan närmar sig det kritiska värdet.

Acknowledgements

First of all, I would like to thank my supervisor Prof. J. Minahan for his helpful advice that allowed me to go through the many difficulties of my first research work. I found the topic he chose inspiring and instructive and finally allowed me to provide some original results. Likewise, I would like to thank all the people that contributed to my interest and knowledge of physics, both in Uppsala and in Torino, which are too many to mention here individually. In particular I am thankful to Anton Nedelin for the interesting discussions and help provided during these months. A great thanks goes to my parents, who encouraged and supported my studies and put my education above everything else. Many are the friends I could count on: thanks to the ones in Torino - Matteo, Lorenzo, Alberto, Sara & Alessandro, Gianmaria & Eleonora, Ilaria & Marco and Eloisa - for keeping such a beautiful relationship despite the distance, and to the ones in Uppsala - Sara & Andrea, Rob & Ana, Frida & Sebastian and Jaume - for the moments spent together and for all the things I learned from them. A special thanks goes to the clubworkers team in GH nation for sharing with me hard work, unforgettable moments and nice beers, and for understanding my struggles with the local language. The last and greatest thanks are for my girlfriend Elisabetta who shared with me these two intense years of learning and personal growth, for always being by my side and for everything we built together.

Contents

Chapter 1

Introduction

The subject of this thesis is the study of the $N = 1^*$ SYM theory on S^5 with matrix model techniques. For this purpose we will first give reviews of matrix models (Chapter 2) and supersymmetry in 5 dimensions (Chapter 3), while Chapter 4 will contain all the original results that are obtained analyzing the theory in its various limits with the appropriate matrix model. In this introductory chapter, on the other hand, we will try to give a more general picture of matrix models, and to explain how they became one of the most useful tools in the study of supersymmetric quantum field theories.

Matrix models have been of interest in theoretical physics since the second half of the 20th century, gaining popularity with Wigner's description of atomic spectra by means of random matrices [1, 2]. According to this model, highly excited energy levels of atoms carried no information about the particular structure of the interactions between the elementary constituents, but were understandable in statistical terms given a suitable statistical ensemble of Hamiltonians. These were large random matrices whose eigenvalues carried information about the level density, level spacing and the transition rates between levels. More recently matrix models found other applications, for example in the study of the discretized $2D$ gravity [3] and the Ising model on random surfaces [3].

The relationship between supersymmetric Wilson loops and matrix models was first pointed out by Erickson, Semenoff and Zarembo [4] in the attempt to verify a prediction from the AdS/CFT correspondence: they showed that under the assumption that a large number of Feynman diagrams (bulk diagrams) cancel off, the expectation value of a circular Wilson loop in the $N = 4$ SYM theory corresponds to the one obtained from a Gaussian matrix model.

The appearence of matrix models in the study of supersymmetric theories is due to localization. Thanks to this mathematical technique the partition function of some particular supersymmetric theories is reduced to a finite integral over the eigenvalues of a certain scalar field (Coulomb moduli). Indeed it was shown by V. Pestun that $N = 4$

SYM on S^4 localizes to a gaussian matrix model, while $N = 2$ and $N = 2^*$ localize to more complicated matrix models [5]. In particular, the partition function obtained by Pestun for $N = 2^*$ SYM is

$$Z = \int d^{N-1}a \prod_{i<j} \frac{(a_i - a_j)^2 H^2(a_i - a_j)}{H(a_i - a_j - M)H(a_i - a_j + M)} e^{\frac{8\pi^2 N R^2}{\lambda} \sum a_i^2} |Z_{inst}|^2 \tag{1.1}$$

where $H(x)$ are some special functions defined as infinite products and $|Z_{inst}|$ is a known, albeit complicated, function of the eigenvalues a_i [6]. It is possible to show that in large N computations the contribution of the instantons is exponentially suppressed, which leads to a great simplification of the integral. From (1.1) the partition functions for $N = 2$ and $N = 4$ SYM can be computed by taking the limits $M \to \infty$ (decoupling of the massive hypermultiplet) and $M \to 0$ (No massive deformation of the N=4 symmetry) respectively. In particular it is clear already from the expression above that $N = 4$ SYM is described by a Gaussian model (See section 2.3.1): in this case the large amount of symmetry is reflected by the reduction of the theory to the simplest known matrix model.

Since then a growing interest arose in this area of research, and localized partition functions were found for theories in diverse dimensions and on various manifolds. These include especially (squashed) spheres §[7], but more exotic geometries have been explored as well [8].

The most interesting quantities that can be computed from a matrix model are the free energy

$$F = -\log Z \tag{1.2}$$

and the expectation value of the supersymmetric Wilson loop

$$W(\mathcal{C}) = \mathrm{Tr}_R P \int_{\mathcal{C}} A_\mu dx^\mu + i\Phi_0 ds \tag{1.3}$$

Among the many interesting results obtained from the study of localized supersymmetric theories, it is worth mentioning the discovery of phase transitions. This kind of behaviour is actually ubiquitous in the large N limit, but the nature of the phase transitions themselves has usually origins that vary strongly from one model to another. A good example of this behaviour was discovered by J. Russo and K. Zarembo in the context of the $N = 2^*$ theory on S^4, which was solved exactly for weak coupling in the decompactification limit, *i.e.* when the radius of S^4 is sent to infinity. In this limit the phase transition occurs in the region between weak and strong coupling, and is caused by the appearence of light resonances in the spectrum of the theory. Analytically, these resonances are responsible for poles in the resolvent that modify its analytical properties at a certain value of the coupling, so that the exact weak coupling solution is not valid

anymore.

In this work the main focus will be on $N = 1$ SYM on S^5. The construction of this supersymmetric theory is due to K. Hosomichi, R. Seong and S. Terashima [9] and it will be reviewed in detail in Chapter 3. Localization, including the computation of one-loop determinants, was performed by J. Källen, J. Qiu and M. Zabzine in [10]. A detailed exposition of the localization techniques requires a lot of technicalities and mathematical sophistication, and is beyond the scope of this thesis; nonetheless we will try to give some picture of the main steps and results in section (3.4) in order to justify the matrix model employed throughout Chapter 4. Most of the research work on this matrix model was done by J. Källen, J. Minahan, A. Nedelin and M. Zabzine: in [11] an extensive study of the case of a single hypermultiplet in the adjoint representation was made, including the computation of the free energy and the expectation value of supersymmetric circular Wilson loops, while in [12] the N^3 behaviour of the free energy at strong coupling is shown. In both cases agreement with the corresponding supergravity calculations is found. This thesis is largely inspired by these papers, since we study the same model with the difference that we use the conventions that the critical hypermultiplet mass is at $\frac{3}{2r}$. In some cases the results that we obtain are just a straightforward generalization of the ones obtained in [11], but in other cases in the proximity of the critical value we find new and peculiar behaviours of the solutions, including a series of phase transitions between the weak and strong coupling regimes.

In our notation, $N = 1^*$ is the specific name for the SUSY theory on S^5 with a single hypermultiplet in the adjoint representation, while $N = 1$ denotes in general SUSY theories that can be constructed on S^5.

Chapter 2

Overview of Matrix Models

In this section we give an introduction to matrix models. In the first part we introduce fatgraphs, which are an extension of normal Feynman diagrams that allow us to keep better track of the N-dependence in the equations. Then we discuss the genus expansion of the free energy and show that it corresponds to a perturbative expansion in $\frac{1}{N}$. In the last section we present the saddle point equation method, that allows us to solve analytically a matrix model in the large N limit, and give an example of this technique. This chaper is largely based on [13], but further references are given in the text.

2.1 Fatgraphs

A matrix model is defined by an action that depends on fields that possess only discrete matrix-element degrees of freedom; the corresponding partition function is given as usual by the path integral

$$Z = \int \mathcal{D}\phi e^{iS[\phi]} \tag{2.1}$$

We consider here the 0-dimensional quantum theory of a gauge field in the adjoint representation. As we will see, this is how a supersymmetric theory looks like after localization. Such a theory is described by a Gaussian matrix model if its partition function has the form

$$Z_G = \frac{1}{Vol(U(N))} \int dM e^{-\frac{1}{2g}\mathrm{Tr}M^2} . \tag{2.2}$$

This model is exactly solvable and its vacuum expactation values (VeVs) can be computed systematically [14]. More complicated models can be studied using perturbation theory around the Gaussian point: for this purpose it is useful to develop a technique that allows us to write down Feynman diagrams that keep track of the matrix structure and of the dependence of the diagrams on the rank of the gauge group N. Such N dependence comes of course from group factors, but a regular Feynman diagram gives rise to a polynomial containing different powers of N. Therefore it is necessary to split

each Feynman diagram into several terms, each one contributing a definite power of N. In order to do this we adopt a double line notation, which consists in replacing propagators in Feynman diagrams with two lines, each carrying one of the two matrix indices. Since the adjoint representation is the tensor product of the fundamental and antifundamental representations, this can be seen as each line carrying an index of the (anti)fundamental representation [13]. The propagator can be found analyzing the free theory with the action

$$S[M] = \frac{1}{2g}\mathrm{Tr}M^2 \tag{2.3}$$

and adding a source term $\mathrm{Tr}JM$ to the action This gives the generating function

$$\Sigma[M] =< e^{\mathrm{Tr}(JM)} > \tag{2.4}$$

whose n^{th} derivative with respect to J gives the n-point correlation function of the theory. A simple expression for $\Sigma[M]$ can be found by completing the square: the action with the source term is

$$-\frac{1}{2g}\mathrm{Tr}M^2 + \mathrm{Tr}JM = -\frac{1}{2g}\mathrm{Tr}(M - Jg)^2 + \frac{1}{2}g\mathrm{Tr}J^2 \tag{2.5}$$

and so we can shift the integration variable, compute the Gaussian integral which gives just an irrelevant numerical coefficient and find

$$\Sigma[M] = e^{\frac{1}{2}g\mathrm{Tr}J^2} \tag{2.6}$$

The propagator is then

$$< M_{ij}M_{kl} >= \frac{\partial}{\partial J_{ji}}\frac{\partial}{\partial J_{lk}}\exp\{\frac{1}{2}gJ_{mn}J_{nm}\}|_{J=0} = g\delta_{jk}\delta_{il} \tag{2.7}$$

which will be represented by the double line

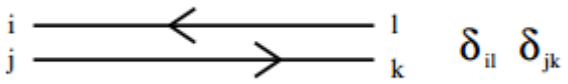

FIGURE 2.1

In a theory with interactions there is also a potential in the Lagrangian, which is a polynomial of the form [13]

$$V(M) = \frac{1}{g}\sum_{p>2}\frac{g_p}{p}\mathrm{Tr}M^p \tag{2.8}$$

The interacting theory is treated pertutbatively around the Gaussian point by using the usual diagrammatic expansion. A vertex with m legs can be represented in the same way, with each leg corresponding to a double line: as an example, let's take the following cubic vertex

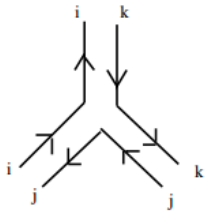

FIGURE 2.2

which corresponds to a factor $\frac{g_3}{g}\mathrm{Tr}M^3$. The fundamental quantities one can calculate are the correlators, which in a quantum field theory with no spacetime degrees of freedom simply correspond to traces of products of matrices. These can be evaluated using Wick's theorem [15] as sums over all the possible pair contractions of the fields in the correlator

$$< \prod_{i,j} M_{ij} >= \sum_{pairings} \prod_{P(i,j)(k,l)} < M_{ij} M_{kl} > \tag{2.9}$$

each of which gives a propagator (2.1) with different indices in the δ-functions. Since each line of the fatgraph carries an index, the different contractions correspond to different ways of joining the lines that come out of two or more vertices. In fact, a single ordinary Feynman diagram corresponds to several fatgraphs, that differ in how the lines coming out of the vertices connect to each other: each of them carries a different power of N, which depends on how the δ_{ij} are contracted with each other. As an example we can consider the loop diagram with two cubic vertices

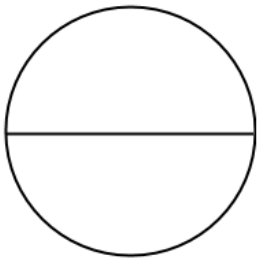

FIGURE 2.3

which gives the correlator

$$< (\mathrm{Tr}M^3)^2 > = \sum_{i,j,k,l,m,n} M_{ij}M_{jk}M_{ki}M_{lm}M_{mn}M_{nl} \tag{2.10}$$

There are the following three inequivalent ways of forming a fatgraph out of this Feynman diagram:

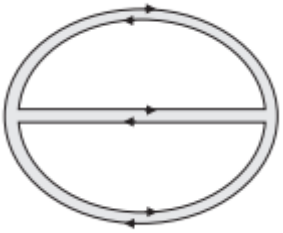

FIGURE 2.4

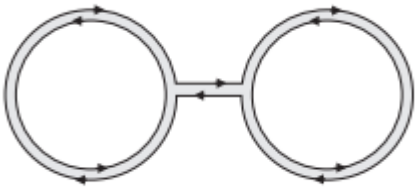

FIGURE 2.5

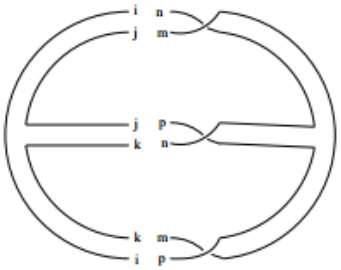

FIGURE 2.6

The first leads to the contraction

$$3 \sum_{i,j,k,l,m,n} < M_{ij}M_{lm} >< M_{jk}M_{nl} >< M_{ki}M_{mn} >= 3gN^3\,. \tag{2.11}$$

The second leads to the contraction

$$9 \sum_{i,j,k,l,m,n} < M_{ij}M_{ki} >< M_{jk}M_{nl} >< M_{lm}M_{mn} >= 9gN^3\,. \tag{2.12}$$

The third leads to the contraction

$$3 \sum_{i,j,k,l,m,n} < M_{ij} M_{lm} >< M_{jk} M_{mn} >< M_{ki} M_{nl} >= 3g^3 N \,, \tag{2.13}$$

where the numeric prefactors in each diagram is a symmetry factor that determines the number of equivalent graphs that give that particular contribution. It is easy to convince ourselves that the power of N that appears in the final result is given by the number of closed lines of the fatgraph [13]: in fact each of them corresponds to a complete contraction of delta functions of the form $\delta_i^j \delta_j^k \dots \delta_n^i = N$.

2.2 The $\frac{1}{N}$ expansion

As we have seen above, the N-dependence is encoded in the topology of the fatgraph. Also the dependence on g and g_p has a topological interpretation: if we regard each fatgraph as a Riemann surface where the propagators correspond to the edges, the loops to the boundaries of the holes, and the total number of vertices is $V = \sum V_p$, we see that each edge E carries a power of g, each vertex V_p carries a power of $\frac{g_p}{g}$, and each hole h carries a power of N. Thus a fatgraph gives a factor

$$g^{E-\sum_p V_p} N^h \prod_p g_p^{V_p} \;=\; g^{E-V} N^h \prod_p g_p^{V_p} \,. \tag{2.14}$$

Making use of the topological relation for the genus G of a surface

$$2G - 2 = E - V - h \tag{2.15}$$

we can rewrite the former equation as

$$g^{2G-2+h} N^h \prod_p g_p^{V_p} = g^{2G-2} t^h \prod_p g_p^{V_p} \,, \tag{2.16}$$

where t is the 't Hooft parameter $t = Ng$. This is particularly useful to compute the perturbative expansion of the free energy $F = -\log Z$, which is given as always by the sum of diagrams corresponding to vacuum connected diagrams [16]. We organize this sum as follows: we sum over all the possible genuses and numbers of holes, and we absorb the dependence on the interaction coupling constants g_p into coefficients $F_{g,h}$, so that

$$F = \sum_{G=0}^{\infty} \sum_{h=1}^{\infty} F_{G,h} g^{2G-2} t^h \tag{2.17}$$

Performing the sum over h, we are left with an expansion in the genuses, which formally defines the free energy at genus G, F_G, by [13]

$$F = \sum_{G=0}^{\infty} F_G(t) g^{2G-2} \tag{2.18}$$

If N is sent to infinity,and g goes to zero in a way that the 't Hooft parameter t is fixed, this can be seen as a perturvative expansion in g or, equivalently, in $\frac{1}{N}$ so that the dependence on N is given by N^{2-2G}:

$$F = \sum_{G=0}^{\infty} F'_G(t) N^{2-2G} \tag{2.19}$$

The leading order of this expansion is given by the diagrams with $G = 0$, the so called planar diagrams, and all the other diagrams give subleading contributions. In the previous example, the two diagrams that gave a N^3 dependence were planar ($G = \frac{E-V-h+2}{2} = \frac{3-2-3+2}{2} = 0$) while the other one was not ($G = \frac{E-V-h+2}{2} = \frac{3-2-1+2}{2} = 1$).

2.3 Saddle point equation

Assuming that our matrices are Hermitian, we have N^2 degrees of freedom. However our matrix model will obviously have the $U(N)$ gauge symmetry corresponding to

$$M \longrightarrow UMU^{\dagger} \tag{2.20}$$

In particular we can use the gauge freedom to diagonalize our matrix, so that we are left with only N degrees of freedom corresponding to the N eigenvalues of the matrix. The gauge fixing procedure is a straightforward application of the Faddeev-Popov method to a theory with no spacetime degrees of freedom, and affects the partition function through the insertion of a factor called "Vandermonde determinant" which is [13]

$$\Delta(\lambda) = \prod_{i<j} (\lambda_i - \lambda_j)^2 \tag{2.21}$$

After this reduction to the eigenvalues the partition function takes the form

$$Z = \frac{1}{N!} \int \prod_{i=1}^{N} \frac{d\lambda_i}{2\pi} e^{-N^2 S_{\text{eff}}(\lambda)} \tag{2.22}$$

with effective action given by

$$S_{\text{eff}} = \frac{1}{tN} \sum_{i=1}^{N} W(\lambda_i) - \frac{2}{N^2} \sum_{i<j} \log|\lambda_i - \lambda_j| \tag{2.23}$$

Since the sum over the N eigenvalues is of order N, the effective action is of order one. Due to the presence of the N^2 prefactor, this means that for large N we can approximate the integral using the saddle-point technique; *i.e.* evaluating it for the field configuration that extremizes the effective action. The saddle point equation, obtained varying the effective action with respect to the eigenvalue λ_i, is then

$$\frac{W'(\lambda_i)}{2t} = \frac{1}{N}\sum_{j\neq i}\frac{1}{\lambda_i - \lambda_j}\,. \tag{2.24}$$

Introducing the eigenvalue distribution function $\rho(\lambda)$ which is defined formally by

$$\rho(\lambda) = \frac{1}{N}\sum_{i=1}^{N}\delta(\lambda - \lambda_i) \qquad \int \rho(\lambda)d\lambda = 1 \tag{2.25}$$

we can rewrite everything in terms of continuous quantities. The saddle point equation becomes

$$\frac{W'(\lambda)}{2t} = \mathrm{P}\int \frac{\rho(\lambda')d\lambda'}{\lambda - \lambda'}\,. \tag{2.26}$$

This is a singular integral equation with Cauchy kernel whose solution is the eigenvalue distribution $\rho(\lambda)$. The integral is defined in the sense of the Cauchy principal value

$$\mathrm{P}\int_a^b = \lim_{\epsilon\to 0}\int_a^{x-\epsilon} + \int_{x+\epsilon}^b \tag{2.27}$$

In this way we have reduced the analytical solution of the matrix model in the planar limit to the study of a Riemann-Hilbert problem. Before showing how this problem is faced, let's make some comments on how the singular integral equation arises. The singular integral comes entirely from the Vandermonde determinant; since it involves a double product over eigenvalues, which results into a double sum when exponentiated, it is responsible of the sum in the saddle point equation which is then turned into an integral. The singularity comes from the differentiation of the logarithmic term in the effective action. Unfortunately, this is a particularly simple case; as we will mention the localization procedure that transforms the partition function of a supersymmetric theory into a matrix integral introduces one-loop determinants into the integral [5] [10]. These factors usually are quite complicated and involve special functions that have a product expression. As a consequence there are tipically more singular terms that lead to more complicated saddle point equations, so that it is not possible to solve the problem with standard techniques. Nontheless sometimes the equations do reduce to the standard case discussed here, and so it is worth exploring in detail.

In order to solve a Riemann-Hilbert problem it is first necessary to define a collection of curves on the complex plane where the eigenvalue density is non-zero; this will determine the general form of the solution. We will concentrate here on the simplest

case, where the density is non-zero only in a connected region $\mathcal{C}$ of the real axis that contains the origin; how this is justified can be seen qualitatively as follows: the effective action can be seen as the action for a system of N point particles, whose coordinates are the eigenvalues λ_i, with no kinetic energy and subject to an attractive central force $W(\lambda_i)$ and a repulsive logarithmic pair interaction [13]. If the pair interaction is weak the particles will be concentrated at the minima of the potential, but spread out if the repulsion is stronger. Our case has a potential with a minimum at the origin and the other minima are irrelevant.

In order to solve the integral equation we introduce the resolvent

$$\omega(x) = \int \frac{dy\rho(y)}{x-y} \tag{2.28}$$

which is an analytic function of x everywhere in the complex plane apart from the interval $\mathcal{C}$ where it has a branch cut. From the normalization of ρ we see that

$$\omega(x) \sim \frac{1}{x}, \quad x \to \infty \tag{2.29}$$

The eigenvalue density is easily expressed in terms of ω; in fact the discontinuity of the resolvent when one crosses the interval $\mathcal{C}$ at y is simply the residue, and so we get

$$\rho(x) = -\frac{1}{2\pi i}(\omega(x+i\epsilon) - \omega(x-i\epsilon)) \tag{2.30}$$

Our singular integral in equation (2.26) is obtained from the resolvent giving an imaginary part to x, so that there are no poles on the real axis. This gives

$$(\omega(x+i\epsilon) + \omega(x-i\epsilon)) = -\frac{1}{t}W'(x) \tag{2.31}$$

which allows us to express the resolvent as the following contour integral around $\mathcal{C}$ [13]

$$\omega(x) = \frac{1}{2t}\oint_{\mathcal{C}} \frac{dz}{2\pi i}\frac{W'(z)}{x-z}\sqrt{\frac{(x-a)(x-b)}{(z-a)(z-b)}} \tag{2.32}$$

This expression allows us to compute the resolvent for any potential $W'(x)$, and the position of the endpoints a and b is then determined imposing the correct behaviour of the resolvent at infinity. However when the potential is a polynomial it is easier to use a more direct approach; from the equation above we see that in this case the residue in $z = x$ just brings out the potential itself, while the singularities at the endpoints can only give a contribution of the form $P(x)\sqrt{(x-a)(x-b)}$ where $P(x)$ is a polynomial of degree $n-1$, where n is the degree of $W'(x)$, with coefficients to be determined. Then

the resolvent has the form

$$\omega(x) = \frac{1}{2t}W'(x) - \frac{1}{2t}P(x)\sqrt{(x-a)(x-b)}\,. \tag{2.33}$$

The $n+2$ parameters $c_0, \dots c_{n-1}, a, b$ can be determined by requiring that the resolvent has the correct behaviour at infinity; in fact expanding the previous expression to order x^{-1} about ∞ and matching with (2.29), we get $N+2$ independent equations which allow us to fix all the parameters.

2.3.1 Gaussian Model

Let's apply the technique described above to the very simple case of the Gaussian matrix model. In this case we have

$$W'(x) = Ax \tag{2.34}$$

and so $P(x)$ is a constant. The resolvent then has the form

$$\omega(x) = \frac{A}{2t}x - \frac{c_0}{2t}\sqrt{(x-a)(x-b)}\,, \tag{2.35}$$

and expanding it around infinity we have

$$\omega(x) = \frac{A-c_0}{2t}x + \frac{1}{4t}(a+b)c_0 + \frac{(a-b)^2c_0}{16tx} \tag{2.36}$$

Requiring that $\omega \sim x^{-1}$ at infinity we get

$$\begin{aligned} c_0 &= A \\ a &= -b \\ a^2 &= \frac{4t}{A} \end{aligned} \tag{2.37}$$

The correct expression for the resolvent is then

$$\omega(x) = \frac{A}{2t}x - \frac{A}{2t}\sqrt{x^2-a^2} \tag{2.38}$$

The eigenvalue distribution is then given by equation (2.30) which in this case becomes

$$\begin{aligned} \rho(x) =& -\frac{1}{2\pi i}(\omega(x+i\epsilon) - \omega(x-i\epsilon)) \\ =& \frac{i}{2\pi}\frac{A}{2t}((x+i\epsilon) - \sqrt{(x+i\epsilon)^2-a^2}) - (x-i\epsilon) + \sqrt{(x-i\epsilon)^2-a^2}) \\ =& \frac{A}{2\pi t}\sqrt{a^2-x^2} = \frac{A}{2\pi t}\sqrt{\frac{4t}{A}-x^2} \end{aligned} \tag{2.39}$$

where we have taken the limit $\epsilon \to 0$ and taken into account that the square root changes sign when crossing the branch cut on the positive real axis. This is the famous Wigner-Dyson distribution which has a semicircular shape.

Chapter 3

Supersymmetry in 5 dimensions

In this chapter supersymmetry in 5 dimensions is introduced, both in flat Euclidean space and on the 5-sphere. This review is based on [9], where an explicit construction of the five dimensional supersymmetric theory on S^5 is provided. A more detailed review is given in [17], where all the algebraic steps are carefully reproduced. We will not discuss supersymmetry in general, and we do not make use of the superfields and superspace formalism. A very good treatment of these topics is given in [18]. In the last section of this chapter we give an outline of how the theory is localized to a matrix model, based on the original calculations presented in [10].

3.1 Euclidean Spinors in 5D

We first consider Euclidean spinors in $\mathbb{R}^5$: there the Γ matrices are a set of 4 x 4 hermitian matrices satisfying

$$\{\Gamma^m, \Gamma^n\} = 2\delta^{mn} \tag{3.1}$$

with an antisymmetrized product denoted by

$$\Gamma^{n_1 n_2 \dots n_p} = \frac{1}{p!}(\Gamma^{n_1}\Gamma^{n_2}\dots\Gamma^{n_p} \pm \dots)\,. \tag{3.2}$$

The Γ matrices in five dimensions are closely related to the 4 dimensional ones; indeed we can take $\Gamma^1 \dots \Gamma^4$ as the Euclidean four dimensional matrices in chiral representation and Γ^5 as the 4-D chirality operator $\Gamma^1\Gamma^2\Gamma^3\Gamma^4$. As in every odd dimensional space a chirality operator cannot be defined, since the product $\Gamma^1\Gamma^2\Gamma^3\Gamma^4\Gamma^5$ turns out to be proportional to the identity. This implies in particular that there are no Weyl spinors. In 5 dimensions the charge conugation matrix is antisymmetric and such that

$$C\Gamma^m C^{-1} = (\Gamma^m)^T = (\Gamma^m)^* \tag{3.3}$$

with the normalization $C^*C = -1$. Majorana spinors cannot be defined in 5 dimensions, since the condition

$$\psi^* = C\psi \tag{3.4}$$

would not respect the consistency relation $(\psi^*)^* = \psi$.

3.2 Vector Multiplets

We now discuss vector multiplets for an arbitrary gauge group on $\mathbb{R}^5$ and see how the Lagrangian and the supersymmetry transformations change if we put the theory on S^5. On flat $\mathbb{R}^5$ a vector multiplet contains a 5-dimensional vector A_m (the gauge field), a real scalar σ, three auxiliary complex scalars D_{IJ} satisfying $D^\dagger_{IJ} = D_{IJ}$ and an $SU(2)_R$ Majorana spinor λ^α_I, where R denotes the R-symmetry, which take values in the Lie algebra of the gauge group. The SUSY variation has the form [9]

$$\begin{aligned}
\delta_\xi A_m &= i\epsilon^{IJ}\xi_I\Gamma_m\lambda_J \\
\delta_\xi\sigma &= i\epsilon^{IJ}\xi_I\lambda_J \\
\delta_\xi\lambda_I &= -\frac{1}{2}\Gamma^{mn}\xi_I F_{mn} + \Gamma^m\xi_I D_m\sigma + \xi_J D_{KI}\epsilon^{JK} \\
\delta_\xi D_{IJ} &= -i(\xi_I\Gamma^m D_m\lambda_J + \xi_J\Gamma^m D_m\lambda_I) + [\sigma, \xi_I\lambda_J + \xi_J\lambda_I]\,,
\end{aligned} \tag{3.5}$$

where the field strength and covariant derivative are defined by

$$\begin{aligned}
F_{mn} &= \partial_m A_n - \partial_n A_m - i[A_m, A_n] \\
D_m\sigma &= \partial_m\sigma - i[A_m, \sigma]\,.
\end{aligned} \tag{3.6}$$

On the other hand on a curved manifold the SUSY parameter cannot be given by a constant spinor, since such objects are generally not well defined. It is instead a Killing spinor that satisfies the Killing equation on S^5

$$D_m\xi_I = \Gamma_m t^J_I\xi_J\,, \tag{3.7}$$

where $t_I{}^J = \epsilon^{JK}t_{IK}$ is a linear combination of Pauli matrices with purely imaginary coefficients such that

$$t_I{}^J t_J{}^K = -\frac{1}{4r^2}\delta_I{}^K\,.$$

For example one can choose

$$t^J_I = \frac{i}{2r}\sigma_3\,. \tag{3.8}$$

Since the SUSY parameter is not constant anymore it will have a non zero variation under the SUSY transformation, and so we will need more terms to make the Lagragian

invariant. The supersymmetry transformations on S^5 become

$$\begin{aligned}
\delta_\xi A_m &= i\epsilon^{IJ}\xi_I\Gamma_m\lambda_J \\
\delta_\xi\sigma &= i\epsilon^{IJ}\xi_I\lambda_J \\
\delta_\xi\lambda_I &= -\frac{1}{2}\Gamma^{mn}\xi_I F_{mn} + \Gamma^m\xi_I D_m\sigma + \xi_J D_{KI}\epsilon^{JK} + 2t_I^J\xi_J\sigma \\
\delta_\xi D_{IJ} &= -i(\xi_I\Gamma^m D_m\lambda_J + \xi_J\Gamma^m D_m\lambda_I) + [\sigma, \xi_I\lambda_J + \xi_J\lambda_I] + i(t_I^K\xi_K\lambda_J + t_J^K\xi_K\lambda_I)
\end{aligned} \tag{3.9}$$

and it can be shown that they leave invariant the Lagrangian

$$\begin{aligned}
\mathcal{L}_{\text{vector}} =& \text{Tr}[\frac{1}{2}F_{mn}F^{mn} - D_m\sigma D^m\sigma - \frac{1}{2}D_{IJ}D^{IJ} + 2\sigma t^{IJ}D_{IJ} - 10t^{IJ}t_{IJ}\sigma^2 + \\
&+ i\epsilon^{IJ}\lambda_I\Gamma^m D_m\lambda_J - \epsilon^{IJ}\lambda_I[\sigma, \lambda_J] - it^{IJ}\lambda_I\lambda_J]
\end{aligned} \tag{3.10}$$

3.3 Hypermultiplet

We present now the matter content of the 5D theory. We will consider only the case which is relevant for our purposes, i.e. a single adjoint hypermultiplet coupled to a $SU(N)$ gauge field. The hypermultiplet contains an $SU(2)_R$ doublet of complex scalars q_I, a fermion ψ and an $SU(2)_R$ doublet of auxiliary scalars F_I. In flat space the Lagrangian

$$\mathcal{L}_M = \epsilon^{IJ}\partial_m\bar{q}_I\partial^m q_J - 2i\bar{\psi}\partial\!\!\!/\psi - \epsilon^{I'J'}F_{I'}F_{J'} \tag{3.11}$$

is invariant under the SUSY transformations

$$\begin{aligned}
\delta_\xi q_I &= -2i\xi_I\psi \\
\delta_\xi\psi &= \epsilon^{IJ}\Gamma^m\xi_I\partial_m q_J + \epsilon^{I'J'}\bar{\xi}_{I'}F_{J'} \\
\delta_\xi F_{I'} &= 2i\bar{\xi}_{I'}\partial\!\!\!/_m\psi
\end{aligned} \tag{3.12}$$

where $\bar{\xi}_{I'}$ is a spinor that satisfies

$$\epsilon^{IJ}\xi_I\xi_J = \epsilon^{I'J'}\bar{\xi}_{I'}\bar{\xi}_{J'} \qquad \xi_I\bar{\xi}_{J'} = 0 \qquad \epsilon^{IJ}\xi_I\Gamma^m\xi_J + \epsilon^{I'J'}\bar{\xi}_{I'}\Gamma^m\bar{\xi}_{J'} = 0 \tag{3.13}$$

whose existence can be easily proven [9]. The coupling to the vector multiplet is realized introducing the covariant derivative

$$D_m\psi = \partial_m\psi - iA_m\psi \tag{3.14}$$

The Lagrangian, after replacing ordinary derivatives with covariant ones, becomes

$$\begin{aligned}
\mathcal{L} =& \epsilon^{IJ}(D_m\bar{q}_I D^m q_J - \bar{q}_I\sigma^2 q_J) - 2(i\bar{\psi}\partial\!\!\!/\psi + \bar{\psi}\sigma\psi) \\
&- i\bar{q}_I D^{IJ}q_J - 4\epsilon^{IJ}\bar{\psi}\lambda_I q_J - \epsilon I'J'\bar{F}_{I'}F_{J'}
\end{aligned} \tag{3.15}$$

which is invariant under the modified transformations

$$\begin{aligned}\delta_\xi q_I &= -2i\xi_I\psi \\ \delta_\xi\psi &= \epsilon^{IJ}\Gamma^m\xi_I D_m q_J + i\epsilon^{IJ}\xi_I\sigma q_J + \epsilon^{I'J'}\bar{\xi}_{I'}F_{J'} \\ \delta_\xi F_{I'} &= 2i\bar{\xi}_{I'}(\not{D}_m\psi + \sigma\psi + \epsilon^{KL}\lambda_K q_L)\end{aligned} \tag{3.16}$$

On a sphere, due to the curvature there is a term proportional to the Ricci scalar of the sphere, which in five dimensions is $\mathcal{R} = \frac{20}{r^2}$, that needs to be taken into account in order to preserve the supersymmetry. Including this term we have the Lagrangian

$$\begin{aligned}\mathcal{L}_{\text{hyper}} =&\epsilon^{IJ}(D_m\bar{q}_I D^m q_J - \bar{q}_I\sigma^2 q_J) - 2(i\bar{\psi}\not{\partial}\psi + \bar{\psi}\sigma\psi) \\ &- i\bar{q}_I D^{IJ}q_J - 4\epsilon^{IJ}\bar{\psi}\lambda_I q_J + \frac{15}{4r^2}\epsilon^{IJ}\bar{q}_I q_J - \epsilon^{I'J'}\bar{F}_{I'}F_{J'}\end{aligned} \tag{3.17}$$

which is invariant under

$$\begin{aligned}\delta_\xi q_I &= -2i\xi_I\psi \\ \delta_\xi\psi &= \epsilon^{IJ}\Gamma^m\xi_I D_m q_J + i\epsilon^{IJ}\xi_I\sigma q_J - 3t^{IJ}\xi_I q_J + \epsilon^{I'J'}\bar{\xi}_{I'}F_{J'} \\ \delta_\xi F_{I'} &= 2i\bar{\xi}_{I'}(\not{D}_m\psi + \sigma\psi + \epsilon^{KL}\lambda_K q_L)\,.\end{aligned} \tag{3.18}$$

We now discuss the mass term for the hypermultiplet; this will be particularly relevant in the following, since we will study our model for values of the mass that deviate slightly from one particular "special point". Mass terms are obtained by giving a vacuum expectation value to the scalar σ in the vector multiplet, so that

$$\begin{aligned}<\sigma> &= \bar{M} \\ <A_m> &= 0 \\ <D_{IJ}> &= -2t_{IJ}\,\bar{M}\,.\end{aligned} \tag{3.19}$$

Collecting all the relevant terms in the Lagrangian, we have

$$\mathcal{L}_{mass} = -\epsilon^{IJ}\bar{q}_I\bar{M}^2 q_J - 2\bar{\psi}\bar{M}\psi + 2it^{IJ}\bar{q}_I\bar{M}q_J + \frac{15}{4r^2}\epsilon^{IJ}\bar{q}_I q_J \tag{3.20}$$

In particular, it is important to notice that the scalar field q_I gets a contribution to its mass from the curvature of the sphere, and so there is an effective mass which is different from the regular mass. The effective mass is given by:

$$\begin{aligned}&-(\frac{15}{4r^2} - \bar{M}^2)\epsilon^{IJ}\bar{q}_I q_J - 2i\bar{M}t^{IJ}\bar{q}_I q_J \\ &= -(\frac{15}{4r^2} - \bar{M}^2)(\bar{q}_1 q^1 + \bar{q}_2 q^2) + \frac{\bar{M}}{r}(\bar{q}_1 q^1 - \bar{q}_2 q^2)\end{aligned} \tag{3.21}$$

which shows that for $\bar{M} = \frac{3}{2r}$ the effective mass of the field q_1 is zero, and in order

to have a stable configuration (negative mass term in the Lagrangian) we can only consider negative fluctuations around this value. For $\bar{M} = -\frac{3}{2r}$ the roles of q_1 and q_2 are interchanged.

3.4 Localization

We give here an outline of how the localization of the supersymmetric theory discussed in the previous sections works. The partition function of the $N = 1^*$ theory with matter on S^5 is

$$Z = \int e^{-S_{\text{vector}} - S_{\text{hyper}}} \tag{3.22}$$

The localization principle states that if we have a symmetry of the action δ_ξ which is not anomalous, and we add to the action an additional term of the form $s\delta_\xi V$, such that $\delta^2 V = 0$, then the partition function of the theory is independent of s. We can then take the limit $s \to \infty$ in order to obtain dramatic simplifications: it is possible to show, indeed, that in this limit, and provided that the bosonic part of $\delta_\xi V$ is positive definite, only the fixed point of δ_ξ contribute to the partition function, together with the one loop determinants that arise from the expansion of the fields about these points. This set of points, called the *localization locus*, is thus given by $\delta_\xi V = 0$ [19]. A suitable term $\delta_\xi V$ was proposed in [9]: this is

$$\delta_\xi \int_{S^5} d^5x \sqrt{g} (\text{Tr}((\delta_\xi \lambda_I)^\dagger \lambda_I) + (\delta_\xi \psi)^\dagger \psi) \tag{3.23}$$

We already have a set of transformations which leaves the action invariant: the SUSY transformations themselves. The fixed points of this term can be found by applying the explicit form of the SUSY transformations (3.9) and (3.18). They are [10], up to complications due to a non-zero instanton number that we will not discuss here,

$$\begin{aligned} A &= 0 \\ \sigma &= \text{constant} \\ D_{IJ} &= -2\sigma t_{IJ} \\ q_I &= 0 \\ F_{I'} &= 0\,. \end{aligned} \tag{3.24}$$

This shows that the infinite dimensional integration in the partition function is reduced to a finite dimensional integral over the constant entries of the matrix σ. In order for localization to be applicable, σ is required to take purely imaginary values [9]. For this reason a new variable $\phi = -ir\sigma$ is introduced, which is real and dimensionless. The remaining task is to calculate the one-loop determinants that give the exact quantum corrections to the localized partition function, which in principle can be done by expanding

around the fixed points up to quadratic order, and then calculating the determinants of Laplace and Dirac operators that result from the Gaussian integral. However this turns out to be a hard task on S^5, and the same result is better achieved using a different approach, that involves putting the SUSY transformations in the so-called *cohomological form* and then using the Atiyah-Singer index theorem to compute the determinants [10]. We will not reproduce this derivation here, and instead we state the result,

$$Z = \int d[\phi] e^{-\frac{8\pi^3}{g_{YM}^2}\mathrm{Tr}\phi^2} \det_{\mathrm{Ad}}(\sin(i\pi\phi) e^{\frac{1}{2}f(i\phi)}) \det_R((\cos(i\pi\phi))^{\frac{1}{4}}) e^{-\frac{1}{4}f(\frac{1}{2}-i\phi)-\frac{1}{4}f(\frac{1}{2}+i\phi)} \tag{3.25}$$

where R denotes the chosen representation for the hypermultiplet and $f(x)$ is a special function that we will investigate more closely in Chapter 4. This is the perturbative partition function, in the sense that by choosing the fixed point $A = 0$ we exclude contributions from topologically nontrivial field configurations. Calculating the instanton partition function is a difficult task, which has not been achieved yet. Nonetheless it is possible to show that these non-perturbative contributions are exponentially suppressed at large N, which is the limit that we are going to consider [10].

Chapter 4

Study of the Matrix Model for $\mathcal{N} = 1^*$ 5D super Yang-Mills

4.1 Matrix Model for $\mathcal{N} = 1^*$ 5D super Yang-Mills

We now present the relevant localized partition function for our model as a function of the t'Hooft coupling $\lambda = g_{YM}^2 N/r$ and the mass parameter $M = ir\bar{M}$. The fields have been normalized so that $\phi_i = -ir\sigma_i$, where σ_i are the eigenvalues of the scalar field σ that belongs to the vector multiplet. The partition function for $\mathcal{N} = 1$ super Yang-Mills on S^5 with gauge group $SU(N)$ and a single hypermultiplet in the adjoint representation, excluding instanton contributions which are suppressed at large N, can be found by adapting to this case the more general expression (3.25) and turning on masses with the help of an auxiliary $U(1)$ vector multiplet [10, 11], and is

$$\begin{aligned} Z \sim \int \prod_{i=1}^{N} d\phi_i \exp(-\frac{8\pi^3 N}{\lambda} \sum_i \phi_i^2 + \sum_{j\neq i} \sum_i (\log(\sinh(\pi(\phi_i - \phi_j))) \\ - \frac{1}{4} l(\frac{1}{2} - iM + i(\phi_i - \phi_j)) - \frac{1}{4} l(\frac{1}{2} - iM - i(\phi_i - \phi_j)) + \frac{1}{2} f(i(\phi_i - \phi_j)) \\ - \frac{1}{4} f(\frac{1}{2} - iM + i(\phi_i - \phi_j)) - \frac{1}{4} f(\frac{1}{2} - iM - i(\phi_i - \phi_j)))) \end{aligned} \tag{4.1}$$

where the functions

$$l(z) = -z \log(1 - e^{2\pi i z}) + \frac{i}{2}(\pi z^2 + \frac{1}{\pi} Li_2 e^{2\pi i z}) - \frac{i\pi}{12} \tag{4.2}$$

$$f(z) = \frac{i\pi z^3}{3} + z^2 \log(1 - e^{-2\pi i z}) + \frac{iz}{\pi} Li_2(e^{-2\pi i z}) + \frac{1}{2\pi^3} Li_3(e^{-2\pi i z}) - \frac{\zeta(3)}{2\pi^2} \tag{4.3}$$

have the important properties [11]

$$l(z) = -l(-z); \quad f(z) = f(-z) \tag{4.4}$$

$$l'(z) = -\pi z \cot(\pi z); \quad f'(z) = \pi z^2 \cot(\pi z) \tag{4.5}$$

and the asymptotic behaviour [11]

$$\begin{aligned}
\lim_{|x|\to\infty} \mathrm{Re} f\left(\frac{1}{2} + ix\right) = -\frac{\pi}{3}|x|^3 + \frac{\pi}{4}|x|\,; \lim_{x\to\infty} \mathrm{Im} f\left(\frac{1}{2} \pm ix\right) = \pm\frac{\pi}{2}x^2\,; \\
\lim_{|x|\to\infty} \mathrm{Re} l\left(\frac{1}{2} + ix\right) = -\frac{\pi}{2}|x|\,; \lim_{x\to\infty} \mathrm{Im} l\left(\frac{1}{2} \pm ix\right) = \mp\frac{\pi}{2}x^2\,; \\
\lim_{|x|\to\infty} \mathrm{Re} f\,(ix) = -\frac{\pi}{3}|x|^3\,; \mathrm{Im} f\,(ix) = 0\,.
\end{aligned}$$

In the large N limit the partition function can be evaluated with the saddle point method. Using the remarkably simple expressions above for the derivatives of $l(z)$ and $f(z)$ we find the equations

$$\begin{aligned}
\frac{16\pi^3 N}{\lambda}\phi_i =& \pi \sum_{j\neq i} [(2 - (\phi_i - \phi_j)^2)\coth(\pi(\phi_i - \phi_j))) \\
&+ \frac{1}{2}(\frac{1}{4} + (\phi_i - \phi_j - M)^2)\tanh(\pi(\phi_i - \phi_j - M)) \\
&+ \frac{1}{2}(\frac{1}{4} + (\phi_i - \phi_j + M)^2)\tanh(\pi(\phi_i - \phi_j + M))]
\end{aligned} \tag{4.6}$$

Taking as usual the continuous limit

$$\frac{1}{N}\sum_{n=1}^{N} \longrightarrow \int_{-\mu}^{\mu} \rho(y)dy$$

we get the singular integral equation

$$\begin{aligned}
\frac{16\pi^2}{\lambda}x =& \int_{-\mu}^{\mu} dy\rho(y)[(2 - (x - y)^2)\coth(\pi(x - y))) \\
&+ \frac{1}{2}(\frac{1}{4} + (x - y - M)^2)\tanh(\pi(x - y - M)) \\
&+ \frac{1}{2}(\frac{1}{4} + (x - y + M)^2)\tanh(\pi(x - y + M))]\,,
\end{aligned} \tag{4.7}$$

where we have assumed that the eigenvalue density $\rho(y)$ is non zero only in a region around the origin. The width of this region, *i.e.* the length of the interval $[-\mu, \mu]$ is determined by the combination of the "central force" term on the left hand side of the equation and the "pair interactions" on the right hand side. In particular for small t'Hooft coupling the eigenvalues are pushed close to each other, while for larger coupling they spread out. However, what the previous statement exactly means in this particular case is not immediately clear due to the complexity of the right hand side of the saddle point equation, and so in the following section original numerical results will be presented in order to justify each possible approximation.

Of fundamental importance is the following: the RHS of equation (4.7) vanishes for the value of the mass $M = \frac{3i}{2}$ which correspond to zero effective mass for the field q_1 (as discussed in section (3.3)). So in this particular case we have the solution $\phi_i = 0$. This means that the free energy of the theory vanishes at $M = \frac{3i}{2}$ for every value of the coupling apart from an irrelevant additive constant, and therefore we will be particularly interested in fluctuations around this special point. We will look at small variations of the mass parameter around the value $M = \frac{3i}{2}$, i.e. we will make the substitution $M \to \frac{3i}{2} - iM$. As discussed in section (3.3), the special value $M = \frac{3i}{2}$ can be approached only from below, and so we will always take small positive values for the parameter M. The tangents in (4.7) get shifted to cotangents, and we get an equation that has poles at $x - y = 0, M, -M$.

After the shift equation 4.7 becomes

$$\begin{aligned}\frac{16\pi^2}{\lambda}x = \int_{-\mu}^{\mu} dy\rho(y)[&(2-(x-y)^2)\coth(\pi(x-y))) \\ &+\frac{1}{2}(\frac{1}{4}+(x-y-\frac{3i}{2}-iM)^2)\coth(\pi(x-y-iM)) \\ &+\frac{1}{2}(\frac{1}{4}+(x-y+\frac{3i}{2}+iM)^2)\coth(\pi(x-y+iM))]\end{aligned} \tag{4.8}$$

This saddle point equation is the main object of study in this chapter. To extract information from it, we will need to make different approximations depending on the relative values of M and $x - y$ corresponding to different values of the coupling λ.

4.2 Numerical Results

In this section we will present the results obtained solving the complete saddle point equation (4.8) numerically with Mathematica. Unless otherwise stated, we have taken $N = 100$, which turns out to be more than enough to justify the large N approximation, and thus the saddle point approach, without being too demanding from the computational point of view. Details about how the numerical calculation has been performed can be found in appendix A. Once all the numerical values of the eigenvalues are known for given M and λ, a number of different quantities can be found: these include their distribution and the free energy of the model. These will be considered later, in order to make comparisons with analytical results. Now we only need to know the order of magnitude of the differences $\phi_i - \phi_j$, and so we will take as an example of this the value of the largest eigenvalue, which we will call μ. Since the distribution is symmetrical around the origin, we have

$$2\mu > |\phi_i - \phi_j| > 0 \tag{4.9}$$

Of course most of the differences $\phi_i - \phi_j$ are much smaller; with the choice $N = 100$, the typical distance between two neighbouring eigenvalues is $\phi_i - \phi_{i-1} \sim \frac{2\mu}{100}$. In the

following tables we report, for a given M, the value of μ for values of λ of increasing magnitude orders

M=10^{-4}	
λ	μ
10^{-4}	$8.5 \cdot 10^{-5}$
10^{-3}	10^{-3}
10^{-2}	$2.2 \cdot 10^{-3}$
10^{-1}	$4.5 \cdot 10^{-3}$
10^{0}	$8.6 \cdot 10^{-3}$
10^{1}	$1.6 \cdot 10^{-2}$
10^{2}	$2.8 \cdot 10^{-2}$
10^{3}	$5 \cdot 10^{-2}$
10^{4}	$9 \cdot 10^{-2}$
10^{5}	$1.8 \cdot 10^{-1}$
10^{6}	1.7

M=10^{-3}	
λ	μ
10^{-4}	$7.7 \cdot 10^{-4}$
10^{-3}	$2 \cdot 10^{-3}$
10^{-2}	$4.7 \cdot 10^{-3}$
10^{-1}	10^{-2}
10^{0}	$2.2 \cdot 10^{-2}$
10^{1}	$4.5 \cdot 10^{-2}$
10^{2}	$8.6 \cdot 10^{-2}$
10^{3}	$1.6 \cdot 10^{-1}$
10^{4}	$3.1 \cdot 10^{-1}$
10^{5}	1.77
10^{6}	18.7

M=0.1	
λ	μ
10^{-4}	$8.6 \cdot 10^{-4}$
10^{-3}	$2.7 \cdot 10^{-3}$
10^{-2}	$8.5 \cdot 10^{-3}$
10^{-1}	$2.6 \cdot 10^{-2}$
10^{0}	$7.7 \cdot 10^{-2}$
10^{1}	0.20
10^{2}	0.52
10^{3}	2.11
10^{4}	18.17
10^{5}	181.81
10^{6}	1818.08

M=0.5	
λ	μ
10^{-4}	$8.5 \cdot 10^{-4}$
10^{-3}	$2.7 \cdot 10^{-3}$
10^{-2}	$8.5 \cdot 10^{-3}$
10^{-1}	$2.7 \cdot 10^{-2}$
10^{0}	$8.5 \cdot 10^{-2}$
10^{1}	0.27
10^{2}	1.04
10^{3}	7.97
10^{4}	78.4
10^{5}	783.7
10^{6}	7837

TABLE 4.1: These tables give the values of μ for different values of the mass of the hypermultiplet M and the coupling constant λ. The results are obtained by solving numerically the complete saddle point equation (4.8) with the software Mathematica for $N = 100$.

The tables above allow us to understand the qualitative behaviour of the solutions of the saddle point equations when the coupling and mass parameter vary. As M increases the eigenvalues tend to be more spread out, especially at strong coupling, but the qualitative behaviour of the solutions basically des not depend on M: they assume larger values when the coupling is larger, in analogy with other simpler matrix models. We can identify five different regions of the parameter space that correspond to different relative values of M, λ and μ and will allow for different approximations of the saddle point equation:

$$\begin{aligned} &\mu \sim M << 1 \\ &\mu << M << 1 \\ &M << \mu << 1 \\ &\mu \sim 1 \\ &\mu >> M >> 1 \end{aligned} \tag{4.10}$$

The dependence of μ on the parameters can be better understood by defining an effective coupling $\lambda_{\text{eff}} = \lambda M$. Doing so, we see that the first three cases correspond to values of $\lambda_{\text{eff}} < 10^2$; this is what we call the weak coupling region.
The last case defines the strong coupling regime; it is already clear from the numerical results that in this case μ grows linearly with λ_{eff}, and this will be confirmed by analytical means in section (4.4).

4.3 Weak coupling regime

Assuming that we are in the weak coupling regime, the eigenvalues will be compressed to a small region around the origin, and so we can assume that $x - y$ and M are small. Then we have

$$\coth \alpha \sim \frac{1}{\alpha} \qquad |x - y \pm iM| << 1 \tag{4.11}$$

and we can approximate the previous expression as

$$\frac{2}{\pi(x-y)} - \frac{1}{\pi(x-y+iM)} - \frac{1}{\pi(x-y-iM)} \tag{4.12}$$

leading to the saddle point equation

$$\frac{16\pi^3}{\lambda} x = \int_{-\mu}^{\mu} dy \rho(y) [\frac{2}{x-y} - \frac{1}{x-y+iM} - \frac{1}{x-y-iM}] \tag{4.13}$$

This equation still allows for different approximations, depending on the respective values of M and $x - y$. We will consider each of them in the next three sections.

4.3.1 Weak coupling: $\mu << M$

If $x - y << M$ the first term dominates the other two, and so our model reduces to the Gaussian model, whose solution we know from section (2.3.1). Examples of the values of λ for which this occurs for a given M can be read from the tables (4.1). In this case we then have the Wigner semicircular distribution for the eigenvalues, which we read

from equation (2.39) with $\lambda = t$ and $A = 16\pi^3$

$$\rho(x) = \frac{8\pi^2}{\lambda}\sqrt{\frac{\lambda}{4\pi^3} - x^2} \tag{4.14}$$

As we can see from the following figure, in this regime the Gaussian model is indeed an excellent approximation of the complete one.

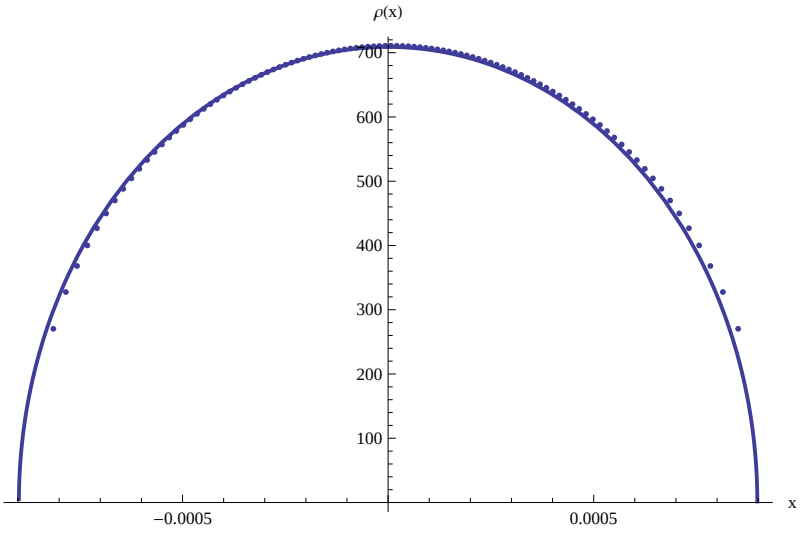

FIGURE 4.1: The countinuous line is the semicircular distribution which solves the Gaussian matrix model, with $\lambda = 10^{-4}$. The dots are the distribution obtained by solving numerically the complete saddle point equation, with $\lambda = 10^{-4}$ and $M = 0.1$. We see that for these values of the parameters the Gaussian model is an excellent approximation to the complete one.

4.3.2 Weak coupling: $\mu >> M$

In the opposite case where $x - y >> M$ the right hand side vanishes, meaning that our approximation is not valid anymore: expanding in powers of M we see that indeed the linear term whose coefficient is $(x-y)^{-1}$ vanishes, and that the next term is

$$-\frac{2M^2}{(x-y)^3} \tag{4.15}$$

We will not discuss in detail this specific case in this thesis, but the saddle point equation

$$Ax = \int_{-\mu}^{\mu} dy \frac{\rho(y)}{(x-y)^3} \tag{4.16}$$

which is then obtained can be reduced by integrating both sides twice to the equation

$$\frac{A}{6}x^3 + Bx = \frac{1}{2}\int_{-\mu}^{\mu} dy \frac{\rho(y)}{x-y} \tag{4.17}$$

whose solution can be found with the standard tecniques introduced in section (2.3), provided that one determines the integration constant B. Numerical solutions for the approximate and for the complete saddle point equations are shown in figure (4.2), confirming the validity of the approximation.

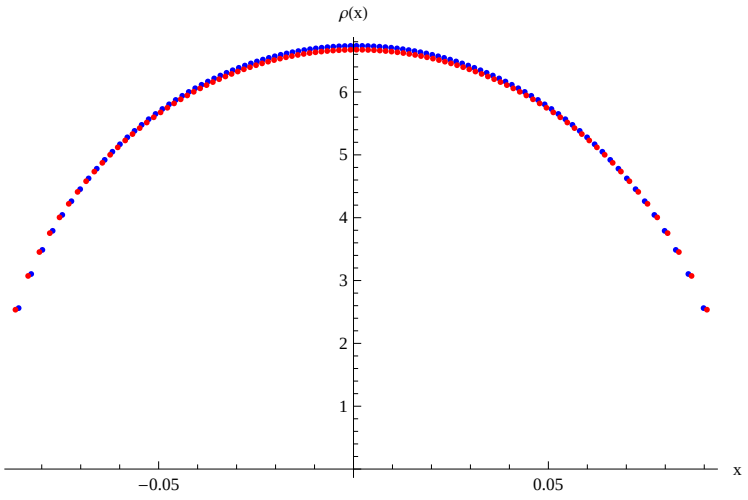

FIGURE 4.2: The red dots represent the eigenvalue distribution obtained by solving numerically the complete saddle point equation for $M = 0.0001$ and $\lambda = 10^4$. The blue dots represent the eigenvalue distribution obtained by solving numerically the saddle point equation with cubic kernel with the same parameters.

4.3.3 Weak coupling: solution of the complete singular equation

If M and $x-y$ are of the same order, we need to study the full equation (4.13). Surprisingly enough, this integral equation has a similar kernel as the one obtained in [20, 21] for the $N = 2^*$ theory on S^4 in the decompactification limit, which we briefly discussed in the intrduction. In our case, however, the LHS is nonvanishing and we have an imaginary mass parameter. This last difference, in particular, is of great importance and leads to a much simpler behaviour of the solution: in fact the kernel in (4.13) has no poles on the real axis, which is where the integration contour lies, and so its analytical properties are much simpler than the one coming from the 4-dimensional theory. In particular, we don't expect to find a phase transtion in this limit. An equation of this kind has been solved by Hoppe [22], and the solution method was reviewed by Kazakov, Kostov and Nekrasov [23]. In the following we will explain and analyze this solution, adapting it to our particular case. For convenience of notation, we absorb the mass parameter into the eigenvalue position by rescaling $x \to Mx$ and defining $\frac{1}{g^2} = \frac{16\pi^3 M^2}{\lambda}$. We also rewrite the kernel as

$$\frac{2}{x-y} - \frac{1}{x-y+i} - \frac{1}{x-y-i} = \frac{2}{(x-y)[(x-y)^2+1]}\,. \tag{4.18}$$

The equation we need to solve is then

$$\frac{x}{g^2} = \int_{-\mu}^{\mu} dy\rho(y)[\frac{2}{(x-y)[(x-y)^2+1]}]\,. \tag{4.19}$$

Our solution will be expressed in terms of the resolvent

$$G(z) = \frac{z^2}{g^2} + \int_{-\mu}^{\mu} dy\rho(y)\frac{1}{(z-y)^2+\frac{1}{4}}\,. \tag{4.20}$$

In fact it can be easily verified that our saddle point equation is equivalent to the equation

$$G(x+\frac{i}{2}) = G(x-\frac{i}{2})\,. \tag{4.21}$$

From the expansion in z around infinity

$$\frac{1}{(z-y)^2+\frac{1}{4}} \approx \frac{1}{z^2} + \frac{2y}{z^3} + \frac{-\frac{1}{4}+3y^2}{z^4}\,, \tag{4.22}$$

we get the asymptotic behaviour for $G(z)$

$$G(z) \approx \frac{z^2}{g^2} + \frac{1}{z^2} + \frac{-\frac{1}{4}+3\nu}{z^4}\,, \tag{4.23}$$

where ν is the second moment of the eigenvalue distribution. Let us now focus on some particular properties of the function G. From the definition we see immediately that

$$G(z) = \bar{G}(\bar{z}) \qquad G(z) = G(-z) \tag{4.24}$$

and that the function has cuts at $(\pm\frac{i}{2}-\mu, \pm\frac{i}{2}+\mu)$. From these properties and provided that the saddle point equation is satisfied, we see that the function is real valued for values of z that lie on the contour shown in figure (4.3), which includes the real axis, the imaginary axis and the two sides of the cut. The function G then defines a map from the region of the 1^{st} quadrant of figure (4.3) outside the contour to the upper half plane. We denote the values of some special points under this map as follows: [23]:

$$\begin{aligned} G(\infty) &= \infty \\ G(0) &= x_1 \\ G(\frac{i}{2}^-) &= x_2 \\ G(\frac{i}{2}+\mu) &= x_3 \\ G(\frac{i}{2}^+) &= x_4 \\ G(+i\infty) &= -\infty \end{aligned} \tag{4.25}$$

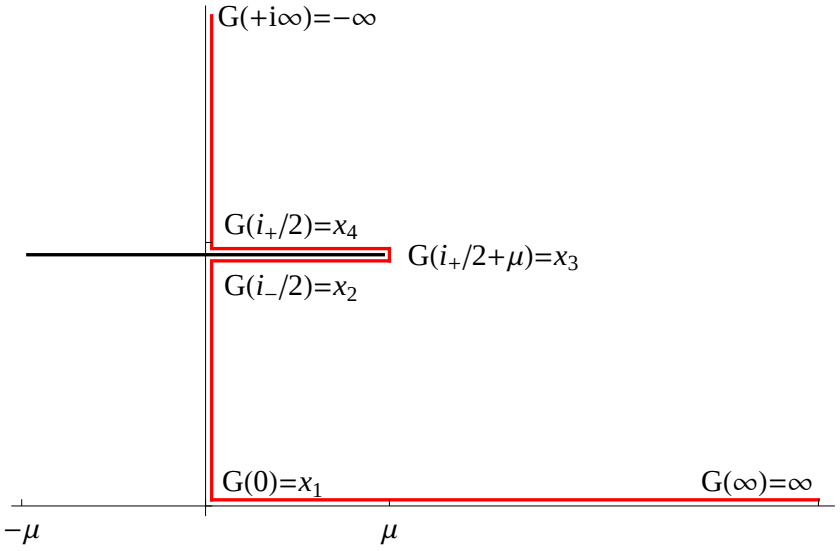

FIGURE 4.3: The contour where the resolvent $G(z)$ is real.

with

$$x_4 < x_3 < x_2 < x_1$$

An expression for the inverse map can be found by looking at the z-plane. Defining $\zeta = G(z)$, we see that between $\zeta = -\infty$ and $\zeta = x_1$ the inverse map has values on the positive real axis. Crossing x_1 we go on the imaginary axis, and so we pick up a phase of $\frac{\pi}{2}$. When we cross x_2 we get another phase of $\frac{\pi}{2}$. When we go around x_3 the real part of the inverse function changes sign, and when finally we pass x_4 we gain another phase of $\frac{\pi}{2}$. A function with these analytical properties is given by the integral

$$z = A \int_{x_1}^{G(z)} \frac{dt(t - x_3)}{\sqrt{(t - x_1)(t - x_2)(t - x_4)}} \tag{4.26}$$

which must then be proportional to the inverse map by analyticity. Carying out the integration along specific portions of the contour separately, we find the following equations that act as conditions on the yet undetermined parameters A, x_1, x_2, x_3, x_4,

$$\begin{aligned} \frac{1}{2} &= A \int_{x_2}^{x_1} \frac{dt(t - x_3)}{\sqrt{(t - x_1)(t - x_2)(t - x_4)}} \\ \mu &= A \int_{x_3}^{x_2} \frac{dt(t - x_3)}{\sqrt{(t - x_1)(t - x_2)(t - x_4)}} \\ \mu &= A \int_{x_4}^{x_3} \frac{dt(t - x_3)}{\sqrt{(t - x_1)(t - x_2)(t - x_4)}} \end{aligned} \tag{4.27}$$

The asymptotic expansion of $z(\zeta)$ is obtained by inverting (4.23)

$$z = g\zeta^{1/2} - \frac{1}{2g}\zeta^{-3/2} - \frac{-\frac{1}{4} + 3\nu}{2g^3}\zeta^{-5/2} \tag{4.28}$$

The same expansion can be obtained by expanding the integrand in (4.26) around $t = \infty$ and performing the integration. The result is

$$\begin{aligned} z \approx\ & 2A\zeta^{1/2} + a_0 + A(2x_3 - x_1 - x_2 - x_4)\zeta^{-1/2} \\ & - \frac{A}{12}(2x_1^2 + 2x_2^2 + 2x_4^2 - 4x_3(x_1 + x_2 + x_4) + (x_1 + x_2 + x_4)^2)\zeta^{-3/2} \\ & - \frac{A}{40}(5x_1^3 + 5x_2^3 + 3x_1^2(x_2 - 2x_3 + x_4) + x_2^2(-6x_3 + 3x_4) + x_2x_4(-4x_3 + 3x_4) \\ & + x_4^2(-6x_3 + 5x_4) + x_1(3x_2^2 - 4x_2x_3 + 2x_2x_4 - 4x_3x_4 + 3x_4^2))\zeta^{-5/2} \end{aligned} \tag{4.29}$$

where a_0 is a constant that we don't need to write down explicitly. Comparing the two results, we get

$$\begin{aligned} A &= \frac{g}{2} \\ a_0 &= 0 \\ x_1 + x_2 + x_4 &= 2x_3 \\ x_1^2 + x_2^2 + x_4^2 - 2x_3^2 &= \frac{6}{g^2} \\ \nu = \frac{M^2}{12} - \frac{g^4}{30}(-\frac{1}{4}(x_1 + x_2 + x_4)(x_1 + x_2 - x_4)^2 &- x_2^2(x_1 + x_2) + x_2(x_1 + x_2)^2) \end{aligned} \tag{4.30}$$

The equations (4.27) can be written in terms of the standard elliptic integrals

$$K(m) = \int_0^{\frac{\pi}{2}} \frac{d\theta}{\sqrt{1 - m\sin^2\theta}} \qquad E(m) = \int_0^{\frac{\pi}{2}} d\theta\sqrt{1 - m\sin^2\theta}\,. \tag{4.31}$$

through a change of variables. In fact if we let

$$\begin{aligned} y_i = gx_i \quad & \lambda_i = \frac{y_i}{y_1 - y_4} \\ m = \frac{y_2 - y_4}{y_1 - y_4} \quad & m' = 1 - \frac{1}{m} \\ \vartheta = \frac{E}{K} \quad E = E(m) \quad & K = K(m) \end{aligned} \tag{4.32}$$

our integral conditions can then be rewritten as [23]

$$\begin{aligned} (y_2 + y_4 - y_1)K(m) + 2(y_1 - y_4)E(m) &= 0 \\ -(y_1 + y_2 - y_4)K(m') + 2(y_2 - y_4)E(m') &= \sqrt{\frac{y_2 - y_4}{g}}\,. \end{aligned} \tag{4.33}$$

From the first equation, by dividing both sides by $y_1 - y_4$, we get an expression for λ_2 as a function of m alone, while the second equation, together with some properties of the elliptic integrals, yields a formula for $y_1 - y_4$. λ_1 and λ_4 are also related to λ_2 in a simple way. The following equalities will the allow us to solve analytically the matrix

model:

$$\begin{aligned} \lambda_2 &= 1 - 2\vartheta \\ \lambda_4 &= \lambda_2 - m \\ \lambda_1 &= \lambda_4 + 1 \\ y_1 - y_4 &= \frac{2}{g\pi^2} K^2 \,. \end{aligned} \tag{4.34}$$

Finally eliminating x_3 in the fourth equation of (4.30) and substituting $x_i = \lambda_i(x_1 - x_4)$ everywhere, we get an expression for $x_1 - x_4$ as a function of λ_2, m and the coupling g

$$\frac{1}{2}(x_1 - x_4)^2(1 - 3\lambda_2^2 - 2\lambda_2 + 4m\lambda_2) = \frac{6}{g^2} \,, \tag{4.35}$$

which together with the previous equation gives

$$\begin{aligned} g^2(m) &= \frac{1}{3\pi^4} K^4(1 - 3\lambda_2^2 - 2\lambda_2 + 4m\lambda_2)) \\ &= \frac{1}{3\pi^4} K^4(-3\vartheta^2 + 2(2-m)\vartheta - (1-m)) \end{aligned} \tag{4.36}$$

From the fifth equation in (4.30) and using the same tricks as above, it is possible to find an explicit expression for the second moment of the eigenvalue distribution;

$$\begin{aligned} \nu &= \frac{1}{12} - \frac{g^4}{30}(-\frac{1}{4}(x_1 + x_2 + x_4)(x_1 + x_2 - x_4)^2) - x_2^2(x_1 + x_2) + x_2(x_1 + x_2)^2 \\ &= \frac{1}{12} - \frac{g^4}{30}(x_1 - x_4)^3(-\frac{1}{4}(\lambda_1 + \lambda_2 + \lambda_4)(\lambda_1 + \lambda_2 - \lambda_4)^2 - \lambda_2^2(\lambda_1 + \lambda_2) + \lambda_2(\lambda_1 + \lambda_2)^2) \\ &= \frac{1}{12} + \frac{1}{15g^2\pi^6} K^6(4m\lambda_2(1-m) + (5\lambda_2^2 - 1)(2m - 1 - \lambda_2)) \\ &= \frac{1}{12} + \frac{K^2}{5\pi^2} \frac{4m\lambda_2(1-m) + (5\lambda_2^2 - 1)(2m - 1 - \lambda_2)}{1 - 3\lambda_2^2 - 2\lambda_2 + 4m\lambda_2} \\ &= \frac{1}{12} - \frac{K^2}{5\pi^2} \frac{10\vartheta^2(\vartheta + m - 2) + 2\vartheta(6 - 6m + m^2) + (1-m)(m-2)}{3\vartheta^2 + 2(m-2)\vartheta + 1 - m} \,. \end{aligned} \tag{4.37}$$

From this procedure it is also clear that taking more terms in the two expansions of $G(z)$ and comparing the coefficients we can find all the even moments of the eigenvalue distribution ($< x^4 >$, $< x^6 > \dots$) as functions of the parameter m. Finally we reintroduce the dependence on the mass parameter M and the coupling λ, getting the following expressions for the coupling and the second moment of the distribution, which are the main result of this section;

$$\lambda(m) = \frac{16M^2}{3\pi} K^4(-3\vartheta^2 + 2(2-m)\vartheta - (1-m)) \tag{4.38}$$

$$\nu(m) = \frac{M^2}{12} - \frac{M^2 K^2}{5\pi^2} \frac{10\vartheta^2(\vartheta + m - 2) + 2\vartheta(6 - 6m + m^2) + (1 - m)(m - 2)}{3\vartheta^2 + 2(m - 2)\vartheta + 1 - m} \tag{4.39}$$

The plots below show λ and ν as functions of m for $M = -0.1$.

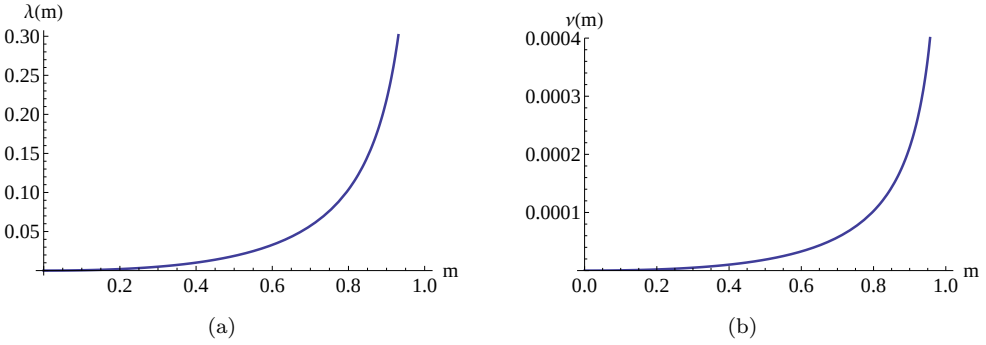

(a) (b)

FIGURE 4.4: The plots show the coupling constant (left) and the second momentum of the eigenvalue distribution (right) as functions of the elliptic parameter m for a mass of the hypermultiplet $M = 0.1$

Moreover ν turns out to be proportional to the derivative of the free energy in the coupling. Defining

$$F = -\log Z \tag{4.40}$$

and recalling that the part of the partition function which involves the coupling is just

$$Z_{quadr} = \int \prod_{i=1}^{N} d\phi_i \exp(-\frac{8\pi^3 N}{\lambda} \sum_i \phi_i^2) = \int \prod_{i=1}^{N} d\phi_i \exp(-\frac{N}{2g^2} \sum_i \phi_i^2) \tag{4.41}$$

we see immediately that

$$\frac{\partial F}{\partial g^2} = -\frac{N^2}{2g^4}\nu = \frac{16\pi^3 N^2 \nu}{\lambda^2} \tag{4.42}$$

We have not been able to find inverse formulae, which are needed in order to express ν as a function of the coupling constant. Nonetheless, for a given value of M, it is possible to determine λ in terms of m, and read off the value of ν at that particular point. This has been done in order to compute analytically the derivative of the free energy with respect to the coupling, using the expression (4.42). We have computed the same quantity by solving numerically the complete saddle point equations. An example of these results is shown in table (4.2), from which we see that the analytical solution of the approximate saddle point equation (4.13) is in good agreement with the numerical results.

$m = 0.1$

λ	$\partial F_{AN}/\partial\lambda$	$\partial F_{NUM}/\partial\lambda$	**Ratio**
1	4366.83	4000.06	1.09
2	2015.72	1804.66	1.12
3	1267.63	1121.61	1.13
4	907.57	797.29	1.14
5	698.42	610.65	1.14
6	562.89	490.62	1.15
7	468.50	407.56	1.15
8	399.29	346.76	1.15
9	346.57	300.70	1.15
10	305.192	264.66	1.15

TABLE 4.2: The table shows the numerical and analytical values of the derivative of the free energy with respect to the coupling for M=0.1 and λ that varies from 1 to 10. In this region the eigenvalues are of order 10^{-1}, and so the use of the approximation (4.13) is justified.

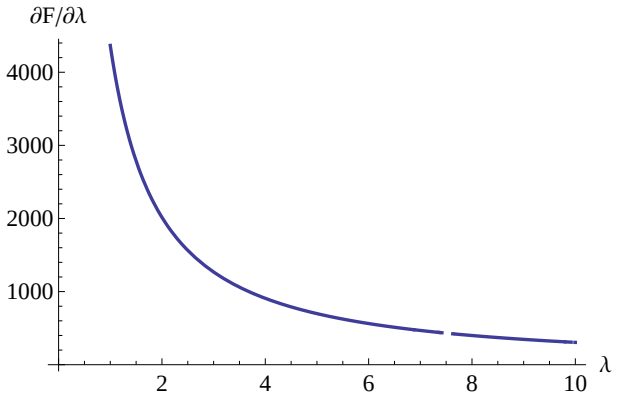

FIGURE 4.5: This plot shows the dependence of $\partial F/\partial\lambda$ on λ. It was obtained inverting (4.38) and substituting it into (4.42)

4.4 Strong Coupling

We now look at how the matrix model behaves for large values of the coupling. A similar calculation has been done in [11] for the same model but around $M = 0$; we will do the same thing around $M = \frac{3i}{2}$. As before the right hand side of the saddle point equation is

$$\begin{aligned}&(2-(\phi_i-\phi_j)^2)\coth(\pi(\phi_i-\phi_j)))\\&+\frac{1}{2}(\frac{1}{4}+(\phi_i-\phi_j-\frac{3i}{2}-iM)^2)\coth(\pi(\phi_i-\phi_j-iM))\\&+\frac{1}{2}(\frac{1}{4}+(\phi_i-\phi_j+\frac{3i}{2}+iM)^2)\coth(\pi(\phi_i-\phi_j+iM))\end{aligned}\tag{4.43}$$

As we discussed in section (4.2), the spread of eigenvalues is determined by λ_{eff}; the strong coupling regime begins when $\lambda_{eff} \sim 10^4$, for which $\mu \sim 10^2$. Using this approximation the equations greatly simplify, since

$$\coth(x-y) \sim \coth(x-y \pm iM) \sim \text{sign}(x-y), \quad x-y >> 1, \quad M << |\phi_i - \phi_j| \,. \tag{4.44}$$

The right hand side then simplifies to

$$\begin{aligned} &\text{sign}(\phi_i - \phi_j)[(2 - (\phi_i - \phi_j)^2) \\ &+ \frac{1}{2}(\frac{1}{4} + (\phi_i - \phi_j - \frac{3i}{2} + iM)^2) + \frac{1}{2}(\frac{1}{4} + (\phi_i - \phi_j + \frac{3i}{2} - iM)^2)] \\ &= M(3-M)\text{sign}(\phi_i - \phi_j) \,, \end{aligned} \tag{4.45}$$

which only depends on the sign of $\phi_i - \phi_j$. The saddle point equation then becomes

$$\frac{16\pi^2 N}{\lambda}\phi_i = -\sum_{j \neq i} M(3-M)\text{sign}(\phi_i - \phi_j) \tag{4.46}$$

Assuming that the eigenvalues are ordered ($\phi_1 < \phi_2 < \cdots < \phi_N$) we get plus signs for $1 \leq j \leq i-1$ and minus signs for $i+1 \leq j \leq N$, which means $i-1$ plus signs and $N-i-1$ minus signs. The sum then gives

$$\sum_{j \neq i} \text{sign}(\phi_i - \phi_j) = (i-1) - (N-i-1) = 2i - N \tag{4.47}$$

and so the saddle point equation has the solution

$$\phi_i = -\frac{M(3-M)\lambda}{16\pi^2 N}(2i - N) \tag{4.48}$$

This shows that the eigenvalues are equally spaced and so we have a constant distribution

$$\begin{aligned} \rho(\phi) &= \frac{8\pi^2}{M\,(3-M)\,\lambda} \quad |\phi| \leq \mu \ , \\ &= \quad 0 \qquad\qquad\quad |\phi| > \mu \ . \end{aligned} \tag{4.49}$$

where μ denotes the largest eigenvalue

$$\mu = \frac{M\,(3-M)\,\lambda}{16\pi^2} \,.$$

When $M \to 0$ we have

$$\mu = \frac{3\lambda_{eff}}{16\pi^2} \tag{4.50}$$

which is always large even when M is very small, coherently with what we stated at the beginning of this section.

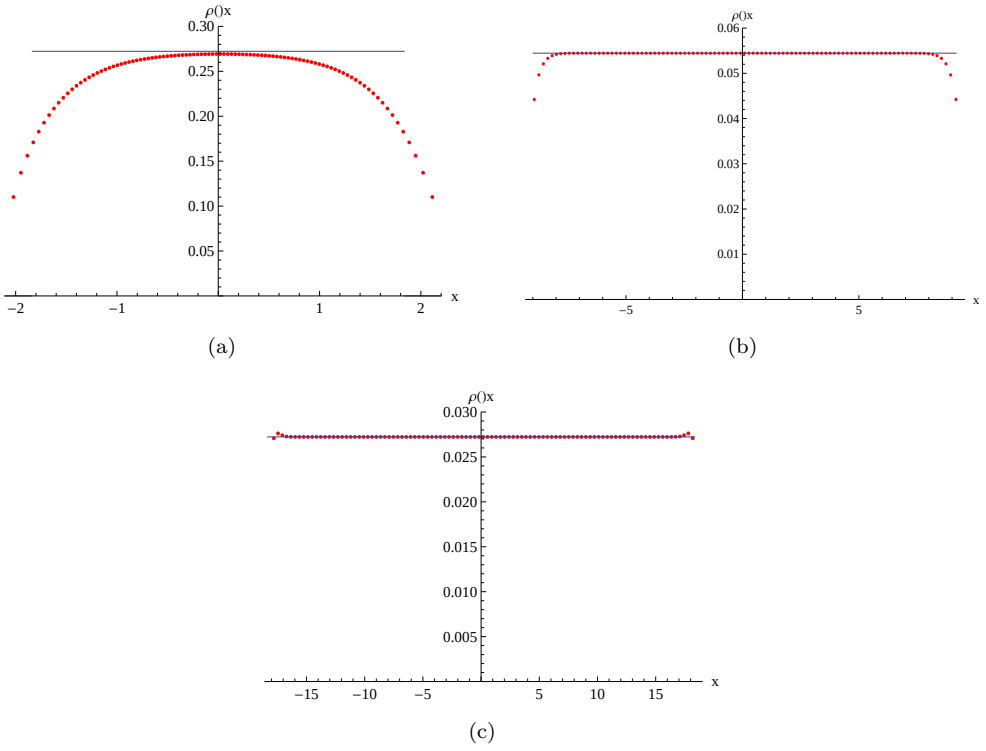

FIGURE 4.6: The three plots show the eigenvalue distribution $\rho(x)$ corresponding to equation (4.46) compared to the one obtained from the numerical solution of the complete saddle point equation for values of the effective coupling $\lambda M = 1000$ (a), 5000 (b) and 10000 (c). We see that the strong coupling approximation starts to be valid for $\lambda M \sim 10^4$

The free energy can be computed exactly. The partition function in the limit of large eigenvalues can be rewritten using the asymptotic expansions (4.6), giving

$$Z \sim \int \prod_i d\phi_i e^{-\frac{8\pi^3 N}{\lambda}\sum_i \phi_i^2 + 2\pi M(3-M)\sum_{j\neq i}\sum_i |\phi_i - \phi_j|} . \tag{4.51}$$

Substituting the solution we found for ϕ_i and using the large-N approximations

$$\sum_{i=1}^{N}(2i-N)^2 \approx \frac{1}{3}N^3 , \qquad \sum_{j\neq i}\sum_{i=1}^{N}|i-j| \approx \frac{1}{3}N^3 . \tag{4.52}$$

we find the following expression for the free energy

$$F = -\log Z = -\frac{g_{YM}^2 N^3}{96\pi r} M\,(3-M)^2 \tag{4.53}$$

This is the same expression found in [11], with a shift in M of $\frac{3i}{2}$, and confirms the remarkable N^3 dependence.

4.5 Study of the small M and fixed effective coupling limit

As we already discussed, in some regions of the parameter space the order of magnitude of the eigenvalues and the different solutions of the saddle point equations are determined by an effective coupling $\bar{\lambda} = \lambda M$, and not by the specific values of λ and M alone. This is basically determined by the fact that the expansion of the right hand side (4.8) of the complete saddle point equations in powers of M starts with the linear term:

$$\begin{aligned}
&(2-x^2)\coth(\pi x) \\
&+\frac{1}{2}\Big(\frac{1}{4}+\big(x-\frac{3i}{2}-iM\big)^2\Big)\coth(\pi(x-iM)) \\
&+\frac{1}{2}\Big(\frac{1}{4}+\big(x+\frac{3i}{2}+iM\big)^2\Big)\coth(\pi(x+iM)) = \\
=&(3\coth(\pi x)-3\pi x\sinh^{-2}(\pi x))M \\
&+(-\coth(\pi x)+\pi(2x-\pi(-2+x^2)\coth(\pi x))\sinh^{-2}(\pi x)M^2 \\
&+O(M^3)
\end{aligned} \tag{4.54}$$

and so when only the first term is relevant we can divide both sides by M, so that our equation becomes

$$\frac{16\pi^2 N}{\bar{\lambda}}\phi_i = \sum_{j\neq i}\left[3\coth(\pi(\phi_i-\phi_j)) - 3\pi(\phi_i-\phi_j)\sinh^{-2}(\pi(\phi_i-\phi_j))\right] . \tag{4.55}$$

This saddle point equation is quite different from the ones we have found before, due to the fact that the kernel on the right hand side is non-singular: the single poles in the

two terms cancel off, so that for small values of the separation $x = \phi_i - \phi_j$ it goes as

$$-3\coth(\pi x) + 3\pi x \sinh^{-2}(\pi x) \approx -2\pi x + O(x^3)\,. \tag{4.56}$$

This is a potential source of problems for the validity of the approximation; infact the second order term in the M expansion comes with a triple pole, so that for small values of the separation between eigenvalues it can become big enough to invalidate the approximation if M is not small enough to compensate. Thus, instead of just requiring $M << 1$, in order to get a meaningful expansion we have to verify that

$$\frac{M}{x^3} << x\,, \tag{4.57}$$

which is a much stricter constraint.

Since we already have solutions in the weak and strong coupling regimes (*i.e.* when the eigenvalues are respectively much smaller and much bigger than one), now we use this approximate equation to extract some information about the "transition" region, where the eigenvalues are of order 1. As we see in section (4.2) this corresponds to an effective coupling $\bar{\lambda} \sim 10^2$. This means that we are free to vary λ and M, as long as their product is constant; we will use this freedom to go to a region of the parameter space where the equation (4.55) is actually a good approximation of the complete one. Since in this region the eigenvalues ar of order 1, the poles can only arise from differences between eigenvalues that are particularly close to each other, and so in order to figure out when the condition (4.57) is valid, we need an estimate of this distance. A good approximation is to take into account the first and second neighbour of each eigenvalue, which leads to the expression

$$< x >= \sum_{i=3}^{N} \frac{|x_i - x_{i-1}| + |x_i - x_{i-2}|}{2N-1}\,. \tag{4.58}$$

The table (4.3) shows that for $M \approx 10^{-8}$ the condition (4.57) is met when $\bar{\lambda} > 10^2$, is still approximately valid when $\bar{\lambda} \sim 50$ and breaks down for smaller values. Since values of $\bar{\lambda}$ much larger than 10^2 correspond to the strong coupling regime that we already investigated thoroughly, in this section we concentrate on smaller values of the coupling and we try to understand how much we can extract from this approximation. In subsection (4.5.1) we present the numerical results, while in subsection (4.5.2) we give analytical explanations of some of these results and try to give some interpretation.

4.5.1 Numerical solutions

The approximate saddle point equation (4.55) can be solved numerically. As displayed in figures (4.11), the solution of the approximate equation is always characterized by

$m = 10^{-8}$		
$\bar{\lambda}$	$< x >$	$\frac{M}{<x>^3}$
100	$4.9{\cdot}10^{-2}$	$8.6 \cdot 10^{-5}$
50	$1.8 \cdot 10^{-2}$	$1.6 \cdot 10^{-3}$
27	$4.6 \cdot 10^{-3}$	$9.6 \cdot 10^{-2}$

TABLE 4.3: The table shows the values of the mean distance between two neighbouring eigenvalues $< x >$ and of the quantity $\frac{M}{<x>^3}$ for various values of $\bar{\lambda}$. In order for equation (4.55) to be valid, the second should be much smaller than the first.

sharp peaks, that seem to increase in number as the coupling increases. This means that the eigenvalues are divided in sets, and eigenvalues belonging to the same set are very close to each other, *i.e.* the distance between them is much smaller than the "natural" distance $\frac{2\mu}{N}$. Moreover, there is a critical value $\bar{\lambda} \sim 25$ under which the only solution allowed is $\phi_i = 0$; we will see in the next section that such critical value can be determined analytically and is $\bar{\lambda}_1 = 8\pi \approx 25.13$.

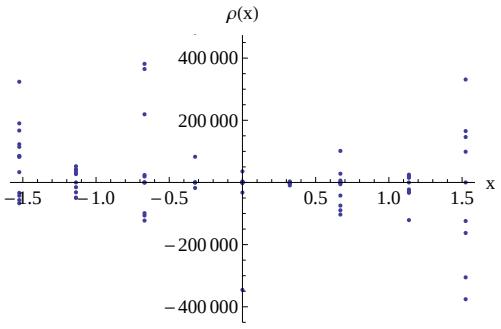

FIGURE 4.7: $\lambda = 100$

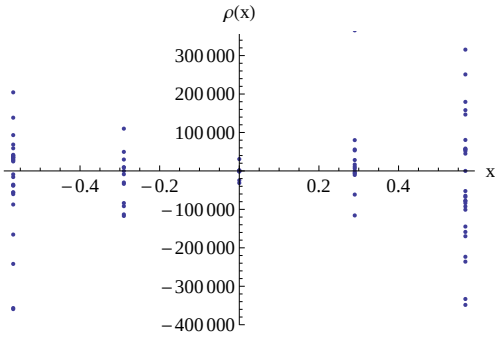

FIGURE 4.8: $\lambda = 50$

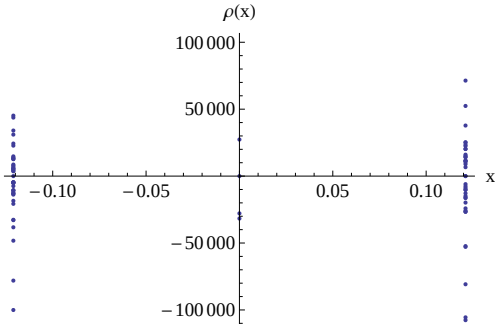

FIGURE 4.9: $\lambda = 27$

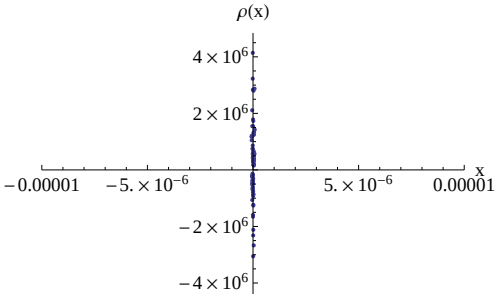

FIGURE 4.10: $\lambda = 25$

FIGURE 4.11: These plots show the eigenvalue distribution $\rho(x)$ obtained from the numerical solution of the approximate saddle point equation (4.55) for various values of the effective coupling $\bar{\lambda}$

Besides, we believe that the numerical analysis only gives us one of several possible solutions that are allowed, the one with the largest possible number of peaks. As a

trivial example, we note that the solution $\phi_i = 0$ is always possible, and so we have to account for it even when the numerical analysis only shows the more complex solution plotted in (4.11). Our conjecture is that there is actually a series of critical values of the coupling $\bar{\lambda}_n$, after which a solution with $2n + 1$ peaks is present together with the ones with a smaller number of peaks, which are allowed also for smaller values of the coupling. As we have seen the first critical value is $\bar{\lambda}_1 = 8\pi$.

So far we haven't checked explicitly whether the solutions of the approximate equations are good approximations of the complete saddle point equations, although as we discussed before table (4.3) together with the condition (4.57) gives us some hints about the region where the approximation is valid. The complete equation depends on both λ and M separately, and so we choose $M \approx 10^{-8}$ so that condition (4.57) is met. Indeed, from figures (4.16) we see that the eigenvalue density obtained from the complete saddle point equation actually has the anomalous peak structure for $\bar{\lambda} = 100$ and $\bar{\lambda} = 50$, although in the second case the solution of the complete equation is smoother. For $\bar{\lambda} = 27$, *i.e.* slightly above the critical point, the approximation can only predict the position ad the number of the peaks, but the solution of the complete equation is clearly a smooth function. For $\bar{\lambda} = 25$, *i.e.* below the critical value, the approximation only gives the zero solution, while the solution of the complete saddle point equation shows an almost semicircular shape, which we can probably identify with the one given by the equation with cubic kernel (4.16) briefly discussed in section (4.3.2). Note that also in this case the approximation predicts correctly the number of peaks of the solution.

4.5.2 Analytical study of the three-peaks case

As we observed in the previous section, the solution where every eigenvalue is zero is allowed for each value of $\bar{\lambda}$. Nonetheless, it is also possible that only some of the eigenvalues are zero, while the other ones are not. We first consider the simplest case, where the eigenavalues are either 0 or $\pm a$, with a to determine analytically. The existence of such a solution for $\bar{\lambda} > 8\pi$ is confirmed by the numerical analysis presented in the previous section, but from that it was not clear if and how this solutions varies by changing the number of zero eigenvalues. We denote by N the total number of eigenvalues, by q the number of eigenvalues at $\pm a$ and by k the number of zero eigenvalues, so that $2q + k = N$. Then the saddle point equations (4.55) reduce to the single equation

$$\begin{aligned}\frac{16\pi^2 N}{\bar{\lambda}} a &= \sum_j 3\coth(\pi(a-\phi_j)) - 3\pi(a-\phi_j)\sinh^{-2}(\pi(a-\phi_j)) \\ &= \sum_{i=1}^{q-1} (3\coth(\pi(a-a)) - 3\pi(a-a)\sinh^{-2}(\pi(a-a)))\end{aligned}$$

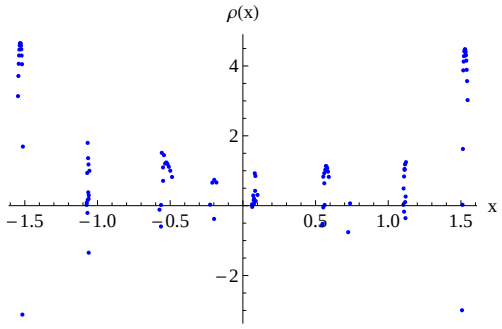

FIGURE 4.12: $\lambda = 100$

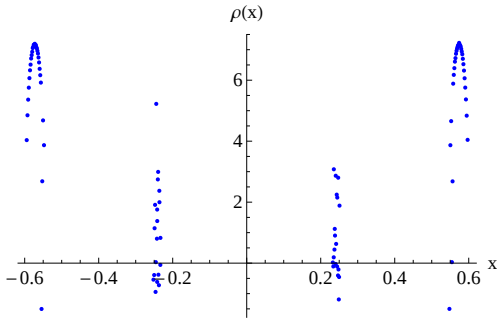

FIGURE 4.13: $\lambda = 50$

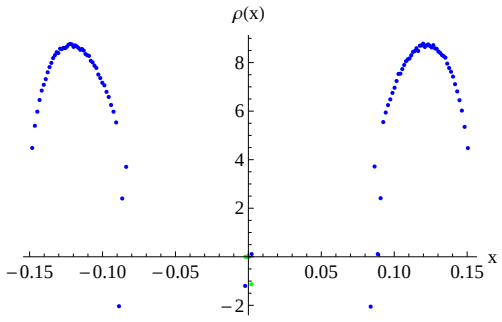

FIGURE 4.14: $\lambda = 27$

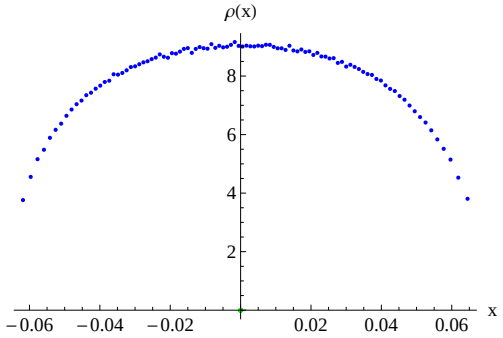

FIGURE 4.15: $\lambda = 25$

FIGURE 4.16: These plots show the eigenvalue distribution $\rho(x)$ obtained from the numerical solution of the complete saddle point equation (4.6) for various values of the effective coupling $\bar{\lambda}$.

$$
\begin{aligned}
&+\sum_{i=1}^{q}(3\coth(\pi(a+a))-3\pi(a+a)\sinh^{-2}(\pi(a+a)))\\
&+\sum_{i=1}^{k}(3\coth(\pi(a))-3\pi(a)\sinh^{-2}(\pi(a)))\\
&=q(3\coth(\pi(2a))-3\pi(2a)\sinh^{-2}(\pi(2a)))+k(3\coth(\pi(a))-3\pi(a)\sinh^{-2}(\pi(a)))\\
&=3(\frac{N-k}{2}(\coth(2\pi a)-2\pi a\sinh^{-2}(2\pi a))-k(\coth(\pi a)-\pi a\sinh^{-2}(\pi a)))
\end{aligned}
\tag{4.59}
$$

since when $\phi_i = -a$ we get the same equation because of the parity properties of the functions involved and when $\phi_i = 0$ the equation is identically satisfied. Equation (4.59) is a trascendental equation in a, and so it needs to be solved numerically (or graphically). However it is possible to understand the qualitative behaviour of the solutions by looking at figure (4.17), where the function

$$
g(a) = \frac{16\pi^2 N}{\bar{\lambda}}a-3(-\frac{N-k}{2}(\coth(2\pi a)-2\pi a\sinh^{-2}(2\pi a))+k(\coth(\pi a)-\pi a\sinh^{-2}(\pi a)))
\tag{4.60}
$$

is plotted for values of the coupling close to the critical point, $N = 100$ and $k = 0$.

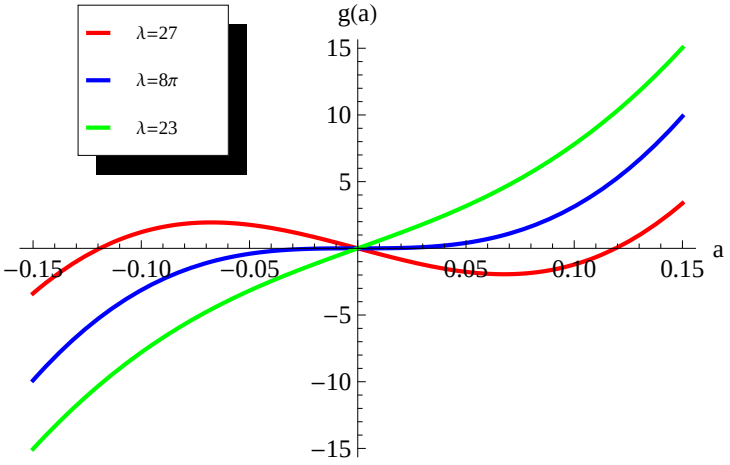

FIGURE 4.17: The function $g(a)$ plotted for values of $\bar{\lambda}$ close to the critical point $\bar{\lambda}_1 = 8\pi$

As we can see in figure (4.18) we don't lose generality with the choice $k = 0$, since increasing the number of zero eigenvalues just causes a small shift of the solutions, but does not change their qualitative dependence on $\bar{\lambda}$. The solutions correspond to the zeros of g: the solution $a = 0$ is always present, while the nonzero solutions are only allowed when the coupling is larger that a certain value $\bar{\lambda}_1$. To determine this value, we notice that the derivative of g at $a = 0$ changes sign when we cross $\bar{\lambda}_1$, and so we look for which value of $\bar{\lambda}$ it is 0.

$$\lim_{a\to 0} \frac{\partial g(a)}{\partial a} = \frac{2N\pi(8\pi - \bar{\lambda})}{\bar{\lambda}} \tag{4.61}$$

and so the critical value is

$$\bar{\lambda}_1 = 8\pi \tag{4.62}$$

We now want to determine the dependence of the free energy on $\bar{\lambda}$ and k. In the planar approximation the free energy is just minus the exponent in the integrand in (4.1), evaluated on the saddle point configuration. Since we are in a limit where λ is very large and M is very small, we can ignore the part of the action quadratic in the fields, since it is proportional to λ^{-1}, and expand the rest in powers of M up to order 1. Then the free energy has the form

$$F = F_0 - F_1 \cdot M + O(M^2) \tag{4.63}$$

where

$$F_0 = \sum_{i\neq j}(3i\pi + \log(2) = N(N-1)(3i\pi + \log(2)) \tag{4.64}$$

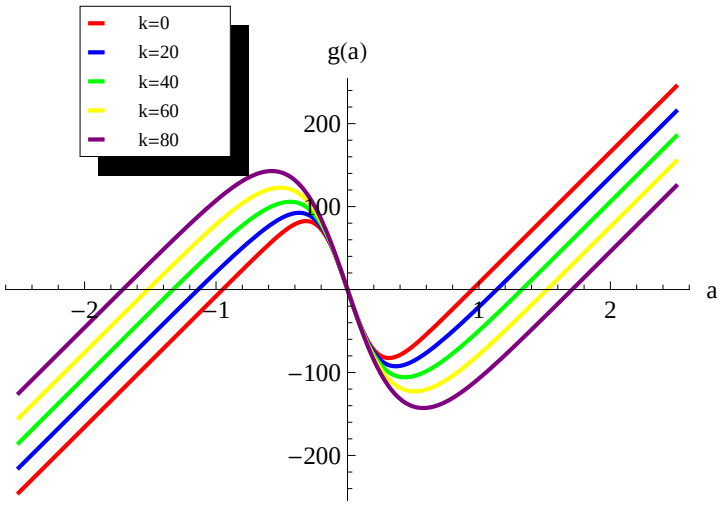

FIGURE 4.18: The function $g(a)$ plotted for values of the number of zero eigenvalues k and $\bar{\lambda} = 100$

is the zero point energy, while the first order contribution turns out to have the simple form

$$F_1 = \sum_{i \neq j} \frac{3}{2} \pi (\phi_i - \phi_j) \coth(\pi(\phi_i - \phi_j)) \,. \tag{4.65}$$

Here we are interested in calculating F_1 in the special case discussed above, where all the eigenvalues are either at $\pm a$ or at 0. The double sum in (4.26) can be calculated as follows:

$$\begin{aligned}
&\sum_{i \neq j} \sum_{j} (\frac{3}{2} \pi (\phi_i - \phi_j) \coth(\pi(\phi_i - \phi_j))) = \\
&= \sum_{i \neq j} (\sum_{i=1}^{k} \frac{3}{2} \pi (\phi_i - 0) \coth(\pi(\phi_i - 0)) + \\
&\quad + \sum_{i=1}^{q} \frac{3}{2} \pi (\phi_i - a) \coth(\pi(\phi_i - a))) + \\
&\quad + \sum_{i=1}^{q} \frac{3}{2} \pi (\phi_i + a) \coth(\pi(\phi_i + a)) = \\
&= \sum_{i \neq j} [\frac{3}{2} k \cdot \pi (\phi_i - 0) \coth(\pi(\phi_i - 0)) + \\
&\quad + \frac{3}{2} q \cdot \pi (\phi_i - a) \coth(\pi(\phi_i - a))) + \\
&\quad + \frac{3}{2} q \cdot \pi (\phi_i + a) \coth(\pi(\phi_i + a))] = \\
&= \frac{3}{2} k(k-1) + \frac{3}{2} q \cdot \pi k \cdot a \coth(\pi a) - \frac{3}{2} q \cdot k \cdot \pi \cdot a \coth(-\pi a) + \\
&\quad + \frac{3}{2} q(q-1) - \frac{3}{2} q^2 \cdot 2\pi \cdot a \coth(-2\pi a) - \frac{3}{2} q \cdot k \cdot \pi \cdot a \coth(-\pi a) + \\
&\quad + \frac{3}{2} q^2 \cdot 2\pi \cdot a \coth(2\pi a) + \frac{3}{2} q(q-1) + \frac{3}{2} k \cdot q \cdot \pi \cdot a \coth(\pi a) =
\end{aligned}$$

$$= \frac{3}{2}\left[2q^2 - 2q + k^2 - k + 4\pi a q^2 \coth(2\pi a) + 4\pi a k q \coth \pi a\right]$$

This expression allows us to calculate F_1 for every value of q and k, once that a is calculated with equation (4.59) for a given $\bar{\lambda}$. Figure (4.19) shows the dependence of F_1 on k for different values of $\bar{\lambda}$, while figure (4.20) shows the dependence of F_1 on $\bar{\lambda}$ for different values of k.

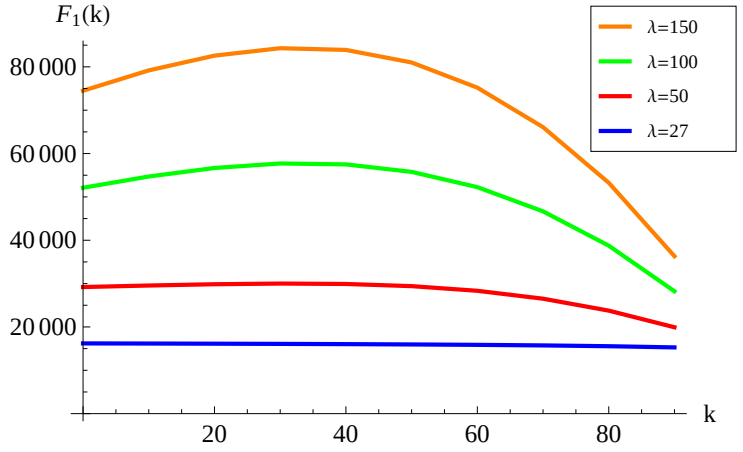

FIGURE 4.19: The function $F_1(k)$ plotted for different values of the effective coupling $\bar{\lambda}$ and $N = 100$

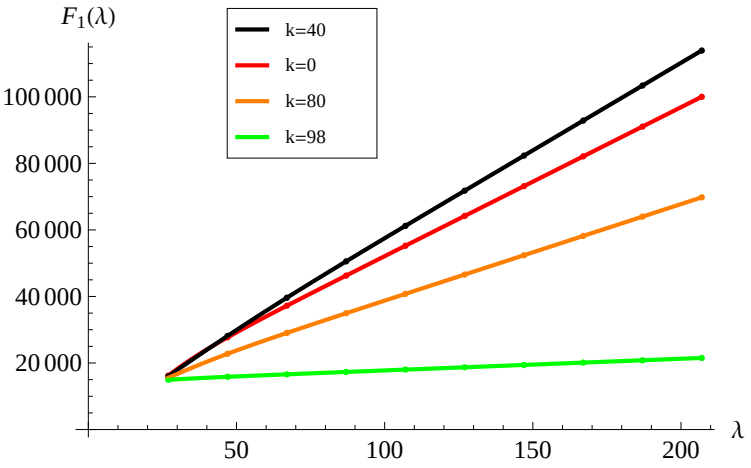

FIGURE 4.20: The function $F_1(\bar{\lambda})$ plotted for different values of the number of zero eigenvalues k and $N = 100$

F_1 grows linearly with $\bar{\lambda}$, while for a given $\bar{\lambda}$ its dependence on k is not monotonic: it grows until k reaches a certain value k_0, and then decreases. For different values of $\bar{\lambda}$ and $N = 100$ we have tried to interpolate $F_1(k)$ with a quadratic function, to see at which k there is a maximum. In each case we get $k_0 \approx 33 \approx \frac{N}{3}$, *i.e.* the eigenvalues are equidistributed between the three peaks.

Similar, although longer, calculations can be performed in the case of five separate peaks. In this case instead of equation (4.59) we get a system of two trascendental equations in the two unknown positions of the peaks a and b; solutions corresponding to the two cohexisting phases with three and five peaks can be found, but we have not been able to determine analytically the second critical value of the coupling, which is found numerically to be $\bar{\lambda}_2 \approx 44.9$

4.5.3 Phase transition

The most interesting result obtained in this section is the peak structure shown in figures (4.11) and (4.16). Analytically, this means that there is a series of critical values of the effective coupling $\bar{\lambda}_n$ after which the complete saddle point equation admitts a solution with a number of cuts larger than one. The interpretation of this is that the system experiences an infinite series of phase transitions as the effective coupling grows, provided that M is small enough so that approximtion (4.55) for the saddle point equation is justified. At this point, it is interesting to understand whether such a phase transition is always present in the intermediate region between weak and strong coupling or if it occurs only when M is very small. We calculated numerically the eigenvalue distributions obtained from the complete saddle point equation for $\bar{\lambda} = 30$ and $\bar{\lambda} = 30$ and increasing values of M. The results of this calculation, shown in figures 4.25 and 4.30, suggest that for M larger than a certain value the two cuts merge so that after a certain treshold there is no phase transition anymore. Something similar is expected to happen also for solutions with a larger number of cuts, which are supposed to merge into each other after certain values of M. Thus, if we keep the product λM fixed and we change M, we can interpret this behaviour as a small-M phase transition. We emphasize however that for larger values of M the effective coupling is not a meaningful quantity anymore, since in that case contributions to the saddle point equation of order 2 in M become relevant.

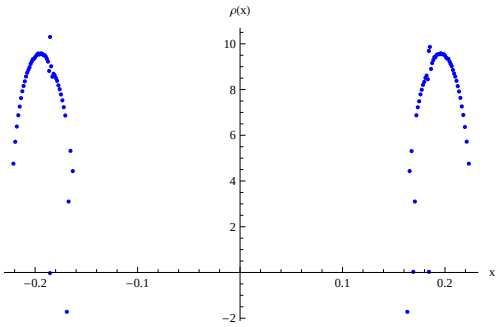

FIGURE 4.21: $M = 10^{-8}$

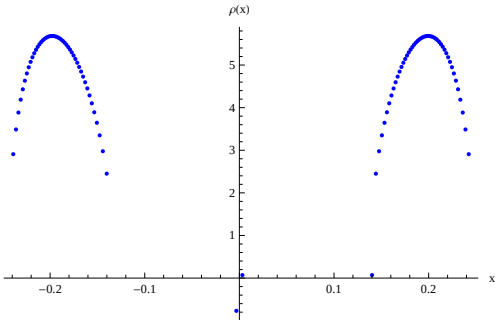

FIGURE 4.22: $M = 10^{-7}$

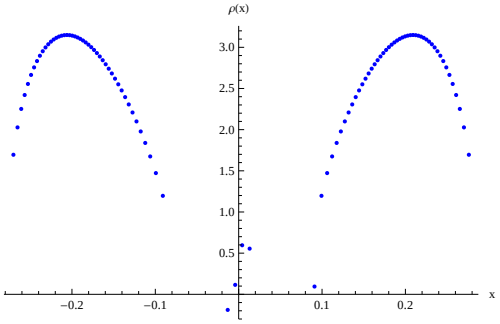

FIGURE 4.23: $M = 10^{-6}$

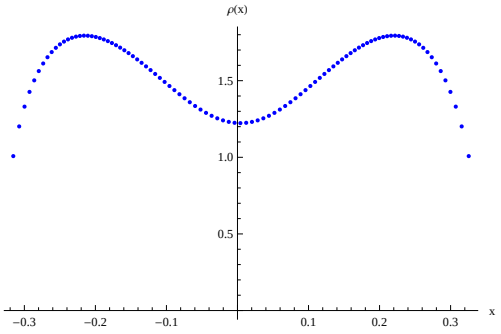

FIGURE 4.24: $M = 10^{-5}$

FIGURE 4.25: These plots show the eigenvalue distribution $\rho(x)$ obtained from the numerical solution of the complete saddle point equation for various values of M and fixed $M\lambda$=30. We see that after a certain value of M the two cuts merge and the system experiences a phase transition.

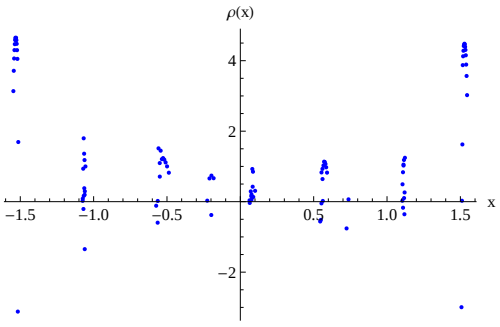

FIGURE 4.26: $M = 10^{-8}$

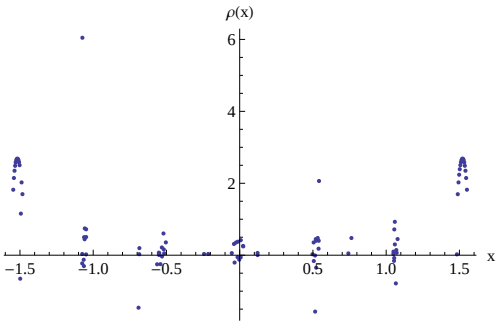

FIGURE 4.27: $M = 10^{-7}$

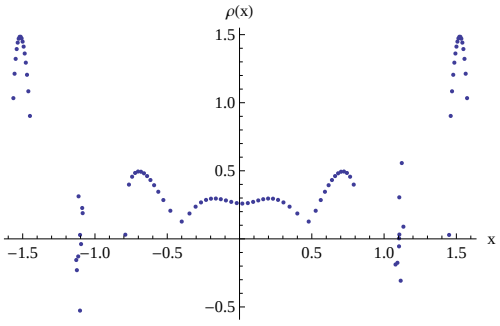

FIGURE 4.28: $M = 10^{-6}$

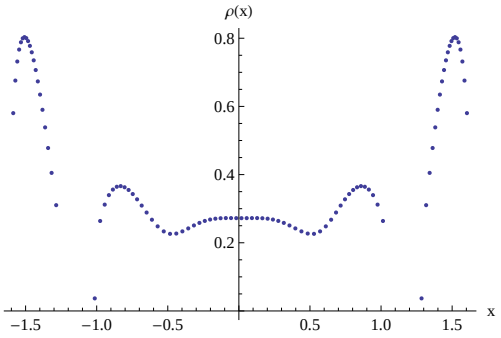

FIGURE 4.29: $M = 10^{-5}$

FIGURE 4.30: These plots show the eigenvalue distribution $\rho(x)$ obtained from the numerical solution of the complete saddle point equation for various values of M and fixed $M\lambda$=100. In this case for small M we have a 7-cut solution. After a certain value of M the peaks merge and the system experiences a phase transition.

Chapter 5

Discussion and outlook

5.1 Discussion

In this thesis we have introduced and discussed thoroughly the matrix model for $N = 1$ SYM on a 5-sphere of radius r in its various limits, and we found analytical solutions in these limits. We have found that there is a critical value of the hypermultiplet mass at $M = \frac{3}{2r}$ for which the effective mass term for one of the scalars in the hypermultiplet in the Lagrangian vanishes. For the same value of the mass the free energy of the model vanishes as well, up to a field independent constant that diverges quadratically in the limit $N \to \infty$. We have then studied the matrix model for values of the mass parameter that approach the critical value from below, making use of different approximations depending on the relative magnitude between the mass parameter and the typical size of the eigenvalues. The use of each approximation is justified by numerical calculations, which also show that we can define weak and strong coupling regimes according to the values of an effective coupling $\bar{\lambda} = \lambda M$. The analytical and numerical results that we presented are original, since previous analysis of this model did not consider the critical mass limit. Most of the results in sections (4.3)-(4.4) are obtained applying well known techniques to this specific problem, while the calculations in section (4.5) are entirely original.

In section (4.3) we have studied the weak coupling case ($\bar{\lambda} << 100$), and depending on whether the mass parameter is much bigger, much smaller or of the same order of the distance between eigenvalues, we have found three different solutions. These are given respectively by the well known Gaussian model, by a model with cubic kernel and by a more complicated model, which was studied by Hoppe and appears also in other related contexts. The exact solution of this model, based on [23], is the most elaborate analytical calculation performed in this thesis. The three different weak coupling solutions correspond to eigenvalue distributions with a similar shape, indicating that we can expect a smooth transition between them when the parameters of the theory are varied.

In section (4.4) the strong coupling limit ($\bar{\lambda} >> 100$) was analyzed, and the solution that we found is a constant distribution which is only a straightforward variation of the one obtained in [11].

In section (4.5) we considered the particular limit where M is very small, so that the saddle point equation of the complete model is approximated by its expansion at first order in M. Due to the presence of singular terms in the expansion, that could in principle invalidate the approximation, we needed to perform a numerical analysis in order to understand in which region of the parameter space the approximation is valid. Inside this region, we chose parameters such that the eigenvalues are of order 1, *i.e.* in the transition region between weak and strong coupling that we could not investigate before. In this limit the eigenvalue distribution shows a peculiar peak structure, with eigenvalues massed around a discrete set of point, symmetrical with respect to the origin. Under a certain critical value of the effective coupling $\bar{\lambda} = 8\pi$, only the solution with eigenvalues all equal to zero is allowed. After that value, a solution with three peaks is allowed as well as the one with one peak at the origin. This pattern continues with a series of critical values of the coupling, after which solutions with a larger number of peaks are allowed. Numerical analysis show that this kind of behaviour is found in the solution of the complete model as well, although in that case the sharp peaks are replaced with smoother curves. We interpreted this as a series of phase transitions that occur when the effective coupling is increased at small M. We found numerically that for fixed $\bar{\lambda}$ the peaks merge and eventually disappear as the mass is increased. In this way we can also interpret this behaviour as a small M phase transition. As we mentioned in the introduction, phase transitions are ubiquitous in gauge theories at large N; nonetheless we are not aware of a case where the phase transition occurs in this particular way.

5.2 Outlook

This thesis contains a comprehensive analysis of the possible approximations to the matrix model for $N = 1^*$ SYM on S^5. Nonetheless there are a few issues that we did not discuss, and that we hope to address in the future.

- In section (4.3.2) we found that in the case $M << x_i - x_j << 1$ the eigenvalue distribution is given by the solution of an integral equation with cubic kernel. We did not work out the solution explicitly, but we suggested a method to reduce this equation to an equation with Hilbert kernel and cubic left hand side, with an undetermined integration constant. If one finds a condition to fix the integration constant, such equation can be solved with standard techniques.

- The solution of Hoppe's equation (4.13) gives analytical expressions for the coupling constant λ and the second moment of the eigenvalue distribution ν as functions of the elliptic parameter m. It would be intersting to invert the expression for $\lambda(m)$ in order to have ν as a function of λ, as well as finding an explicit expression for the largest eigenvalue μ. Similar calculations have been done in [21] for the theory on S^4 employing Jacobi Θ-functions and Eisenstein series. It is possible that a similar approach can be used in this context.

- It would be of great interest to have some more analytical results about the region of parameter space where the eigenvalues are of order one, in order to understand better the nature of the phase transition discussed in section (4.5.3). The approach followed in section (4.5.2) is probably not too hard to generalize to a larger number of peaks, in order to have analytical results for the free energy in the various phases.

- It is possible to consider the localized Chern-Simons theory on S^5, which differs from the one discussed here for an additional cubic term in the action. This has been done in [24], showing that the theory presents a rich phase structure. It would be interesting to analyze the behaviour of the same matrix model around the critical point $M = \frac{3}{2r}$, as we did here, and see how this shift affects the phase structure of the theory.

Moreover there are some general issues that we did not address, which are of great importance for a better understanding of SUSY theory on S^5 itself and its possible applications:

- SUSY theories in 5D are non-renormalizable, as can be inferred from general principles and confirmed by explicit calculations [25]. Nonetheless localization seems to be well defined and not affected at all by this problem; how this is possible is currently not understood.

- As we mentioned, localization gives only an expression for the perturbative partition function. The complete partition function must include the contributions from instantons, which have not been calculated so far.

- One of the main reasons to study a 5D SYM theory is its relation with the mysterious 6D (2,0) superconformal theory, which does not possess a Lagrangian description and is mainly known through its conjectured AdS_7 dual. Interesting results on this topic have been obtained in [12] and [11]; it is unclear whether this thesis can give new insights on this problem or not.

Appendix A

Numerical Methods

In this appendix we will explain how the numerical results presented in this work are obtained. The most important application of numerical tecniques in this thesis is the solution of the complete saddle point equation 4.6, or its shifted version where $M \to \frac{3i}{2} - M$. As explained throughout Ch. 4, this is needed both to determine which approximation can be used in order to find a simplified analytic solution and to check the validity of the approximate solution itself. Expression 4.6 is a system of N equations in N unknowns, whose use is legitimate only in the large N limit, where the partition function 4.1 can be approximate by the value of the integrand at the saddle point. The N equations, in their shifted version, are written in a compact form as functions of the coupling constant λ and the mass of the hypermultiplet M using the following Mathematica code:

```
Equations[M_, \[Lambda]_,N_] :=
  Table[16 Pi^2 N/\[Lambda]  Subscript[x, i] -
    Total[Table[((2 - (Subscript[x, i] -
              Subscript[x, j])^2) Coth[\[Pi] (Subscript[x, i] -
              Subscript[x, j])] +
         1/2 (1/4 + (-((3 I)/2) -
              I M + (Subscript[x, i] -
                Subscript[x, j]))^2) Tanh[\[Pi] (-((3 I)/2) -
              I M + (Subscript[x, i] - Subscript[x, j]))] +
         1/2 (1/4 + ((3 I)/2 +
              I M + (Subscript[x, i] -
                Subscript[x, j]))^2) Tanh[\[Pi] ((3 I)/2 +
              I M + (Subscript[x, i] - Subscript[x, j]))]), {j, 1,
        i - 1}]] -
    Total[Table[((2 - (Subscript[x, i] -
              Subscript[x, j])^2) Coth[\[Pi] (Subscript[x, i] -
              Subscript[x, j])] +
         1/2 (1/4 + (-((3 I)/2) -
              I M + (Subscript[x, i] -
                Subscript[x, j]))^2) Tanh[\[Pi] (-((3 I)/2) -
              I M + (Subscript[x, i] - Subscript[x, j]))] +
         1/2 (1/4 + ((3 I)/2 +
              I M + (Subscript[x, i] -
```

```
              Subscript[x, j]))^2) Tanh[\[Pi] ((3 I)/2 +
            I M + (Subscript[x, i] - Subscript[x, j]))]), {j, i + 1,
        N}]], {i, 1, N}];
```

The command `Total[Table` is the most efficient way to define sums. It is necessary to split the sum over j in two pieces to take into account that $j \neq i$. Since these equations are trascendental, they cannot be solved using the command `NSolve`, but the command `FindRoot` is needed instead. The complete command is

```
Sol[M_,\[Lambda]:,N_]:=
 FindRoot[Equations[M, \[Lambda]],
  Table[{Subscript[x, i], i}, {i, 1, N}]];
```

where the `Table` is only used to specify a different value from which to start the research of the root x_i for each i, since the command `FindRoot` does not allow to specify identical initial starting values for the roots. Once the eigenvalues x_i are calculated, the distribution can be plotted using the following commands:

```
solutions = Sol[M,\[Lambda]]

data =
  Table[{Subscript[x, i] /. solutions,
    1/(N (Subscript[x, i] - Subscript[x, i - 1])) /.
     solutions}, {i, 2, N}];

plot = ListPlot[data]
```

We found that $N \sim 100$ is the best choice, since it gives an excellent approximation of the large N limit without being too demanding from the computational point of view. A larger N is however more appropriate for eigenvalue distributions which present several peaks, since a larger number of points allows to recognize better the shape of each peak.

Bibliography

[1] Eugene P. Wigner. Random matrices in physics. 9(1):1–23, January 1967. ISSN 0036-1445 (print), 1095-7200 (electronic). URL `http://link.aip.org/link/siread/v9/i1/p1/s1;http://www.jstor.org/stable/2027409`.

[2] E. P. Wigner. Characteristic Vectors of Bordered Matrices With Infinite Dimensions. *The Annals of Mathematics*, 62(3):548–564, 1955. URL `http://www.jstor.org/stable/1970079`.

[3] P. Di Francesco, Paul H. Ginsparg, and Jean Zinn-Justin. 2-D Gravity and random matrices. *Phys.Rept.*, 254:1–133, 1995.

[4] J.K. Erickson, G.W. Semenoff, and K. Zarembo. Wilson loops in N=4 supersymmetric Yang-Mills theory. *Nucl.Phys.*, B582:155–175, 2000.

[5] Vasily Pestun. Localization of gauge theory on a four-sphere and supersymmetric Wilson loops. *Commun.Math.Phys.*, 313:71–129, 2012.

[6] Nikita A. Nekrasov. Seiberg-Witten prepotential from instanton counting. *Adv.Theor.Math.Phys.*, 7:831–864, 2004.

[7] Jun Nian. Localization of Supersymmetric Chern-Simons-Matter Theory on a Squashed S^3 with $SU(2) \times U(1)$ Isometry. *JHEP*, 1407:126, 2014.

[8] Jian Qiu, Luigi Tizzano, Jacob Winding, and Maxim Zabzine. Gluing Nekrasov partition functions. 2014.

[9] Kazuo Hosomichi, Rak-Kyeong Seong, and Seiji Terashima. Supersymmetric Gauge Theories on the Five-Sphere. *Nucl.Phys.*, B865:376–396, 2012.

[10] Johan Källén, Jian Qiu, and Maxim Zabzine. The perturbative partition function of supersymmetric 5D Yang-Mills theory with matter on the five-sphere. *JHEP*, 1208:157, 2012.

[11] Joseph A. Minahan, Anton Nedelin, and Maxim Zabzine. 5D super Yang-Mills theory and the correspondence to $\mathrm{AdS}_7/\mathrm{CFT}_6$. *PoS*, EPS-HEP2013:544, 2013.

[12] J. Kallen, J.A. Minahan, A. Nedelin, and M. Zabzine. N^3-behavior from 5D Yang-Mills theory. *JHEP*, 1210:184, 2012.

[13] Marcos Marino. Les Houches lectures on matrix models and topological strings. 2004.

[14] P. Di Francesco and C. Itzykson. A Generating function for fatgraphs. *Annales Poincare Phys.Theor.*, 59:117–140, 1993.

[15] M. Marino. Chern-Simons theory, matrix models, and topological strings. *Int.Ser.Monogr.Phys.*, 131:1–197, 2005.

[16] M. Srednicki. *Quantum field theory.* 2007.

[17] D. Keijdener. Localization and its application to N=1 Super Yang-Mills theory with matter on the 5-sphere. 2013.

[18] Jonathan Bagger and Julius Wess. Supersymmetry and supergravity. 1990.

[19] Marcos Marino. Lectures on localization and matrix models in supersymmetric Chern-Simons-matter theories. *J.Phys.*, A44:463001, 2011.

[20] J.G. Russo and K. Zarembo. Massive N=2 Gauge Theories at Large N. *JHEP*, 1311:130, 2013.

[21] Jorge G. Russo and Konstantin Zarembo. Evidence for Large-N Phase Transitions in N=2* Theory. *JHEP*, 1304:065, 2013.

[22] J. Hoppe. QUANTUM THEORY OF A RELATIVISTIC SURFACE. 1986.

[23] Vladimir A. Kazakov, Ivan K. Kostov, and Nikita A. Nekrasov. D particles, matrix integrals and KP hierarchy. *Nucl.Phys.*, B557:413–442, 1999.

[24] Joseph A. Minahan and Anton Nedelin. Phases of planar 5-dimensional supersymmetric Chern-Simons theory. 2014.

[25] Zvi Bern, John Joseph Carrasco, Lance J. Dixon, Michael R. Douglas, Matt von Hippel, et al. D = 5 maximally supersymmetric Yang-Mills theory diverges at six loops. *Phys.Rev.*, D87:025018, 2013.